Supplementary Information

Molecular structural engineering of donor-acceptor-based porous organic polymers for sulfide photooxidation in water: A sustainable approach

Neha Saini, Kirti Dhingra, Amit Kumar and Kamalakannan Kailasam*

Advanced Functional Nanomaterials, Institute of Nano Science and Technology (INST), Knowledge City, Sector-81, Manauli, SAS Nagar, 140306 Mohali, Punjab, India.

***Email:** kamal@inst.ac.in*

Instrumentation

Bruker Vertex FT-IR 70/80 spectrometer was used for Fourier-transform infrared spectroscopy (FTIR) analysis in the spectral range of 4,000-400 cm^{-1}. ^{13}C cross-polarization magic angle spinning (CP/MAS) solid-state nuclear magnetic resonance (NMR) was recorded on a Bruker Avance NEO 400 using a 5 mm FG NMR probe. The products of catalytic reactions were identified, and the catalytic conversions were determined by ^{1}H NMR spectra and recorded in $CDCl_3$ on a Bruker Avance NEO 400 spectrometer operating at a frequency of 400 MHz. UV/Vis diffuse reflectance spectra (DR UV/Vis) measurements were carried out on Agilent Cary 100 UV-Vis spectrophotometer. X-ray diffraction (XRD) pattern of the powder samples were recorded on Bruker D8 Advance diffractometer equipped with a scintillation counter detector with a Cu Kα radiation (λ = 0.15418 nm) source operating at 40 kV and 40 mA. SHIMADZU DTG-60H analyzer was used to perform the thermogravimetric analysis (TGA) under the N_2 environment (flow rate of 20 mL/min) in the temperature range of 30 to 900 °C with a ramping rate of 10 °C/min. Field emission scanning electron microscopy (FESEM) was employed to analyze the morphology of the samples recorded using the JEOL JSM-7610F Plus instrument. Nitrogen physisorption isotherms were recorded at 77 K using an Autosorb iQ3 instrument (Quantachrome). Before carrying out the analysis, all the samples were degassed at 150 °C for 24 h. Micropore BET assistance method was used to determine the surface area of synthesized polymeric networks. X-ray photoelectron spectroscopy (XPS) was used to determine the sample's chemical states and elemental compositions in an ultra-high vacuum environment using an Al Kα X-ray source and a monochromator (Thermo Fisher

Scientific). Photoluminescence spectra (PL) and lifetime measurements were carried out using Horiba Fluorolog instrument. Water contact angle measurements were performed using a drop-shape analysis apparatus (DSA25 Drop Shape Analyzer, KRÜSS GmbH). EPR analysis was carried out using Bruker A300-9.5/12/S/W at room temperature. The quantification of gaseous H_2 was performed by Shimadzu Gas Chromatography (GC 9790 Instruments) equipped with a thermal conductive detector (TCD) and argon (Ar) as a carrier gas. The electrochemical investigations were conducted utilizing a Metrohm Autolab M204 multichannel potentiostat galvanostat. The determination of the conduction band was accomplished utilizing Mott-Schottky electrochemical measurements. For sample preparation, a fine paste was obtained by dispersing the sample in ethanol and nafion, followed by drop-casting onto a glassy carbon electrode (GCE) and subsequent overnight drying. Electrochemical impedance spectra measurements were performed employing a three-electrode system, where a platinum wire was employed as the counter electrode and an Ag/AgCl (3 M KCl) reference electrode was used.

Photoelectrochemical measurements

For the photoelectrochemical measurement, 2 mg of the sample was dispersed into 0.2 mL of ethanol and ultrasonicated for 30 min. This prepared homogeneous solution was then drop casted on ITO in a 0.5x0.5 cm^2 area. The LSV studies and photocurrent measurements with 30 s (on/off) light cycles were carried out using an Autolab electrochemical workstation with three-electrode configurations and 400 W Xenon lamp.

Synthesis

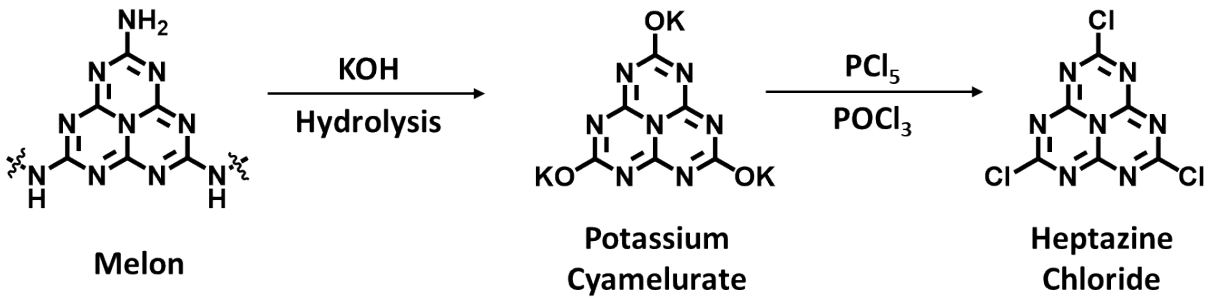

Synthesis of 2,5,8-tris(potassium)cyamelurate:

5 g of 2,5,8-tris(potassium)cyamelurate was taken into a 250 mL round bottom flask containing 100 mL of 3 M KOH solution followed by reflux for 6 h at 140 °C. When the solution became clear, it was filtered and allowed to cool at room temperature. White precipitates of 2,5,8-tris(potassium)cyamelurate are formed and washed with cold ethanol and allowed to dry overnight at 80 °C.

Synthesis of Heptazine Chloride (Cyameluric Chloride):

A mixture of 2,5,8-tris(potassium)cyamelurate (3 g) and phosphorous pentachloride (10 g) was refluxed in 40 mL phosphorous oxychloride at 140 °C for 6 h. The solution turned yellow coloured and was cooled at room temperature and filtered. This solution was rota evaporated to obtain yellow precipitates of Heptazine chloride (Yield= 56%). ^{13}C NMR (in d-THF) = 174.9 and 158.1 ppm. FTIR (ATR, cm^{-1}): 1600, 1500, 1295, 1200, 1086 938, 822, 645

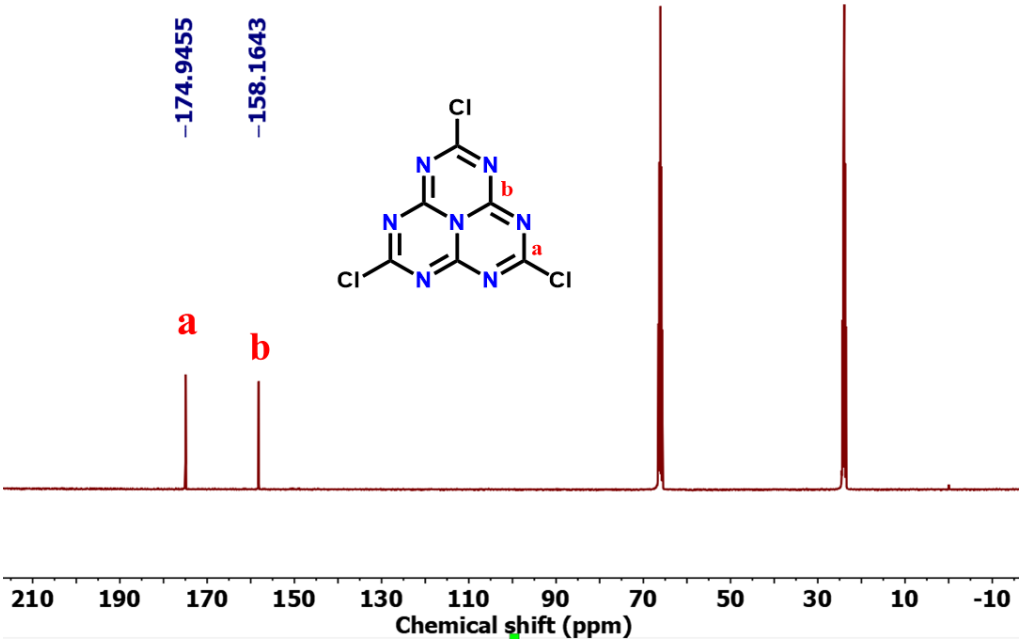

Fig. S1 ^{13}C NMR spectrum of Heptazine Chloride.

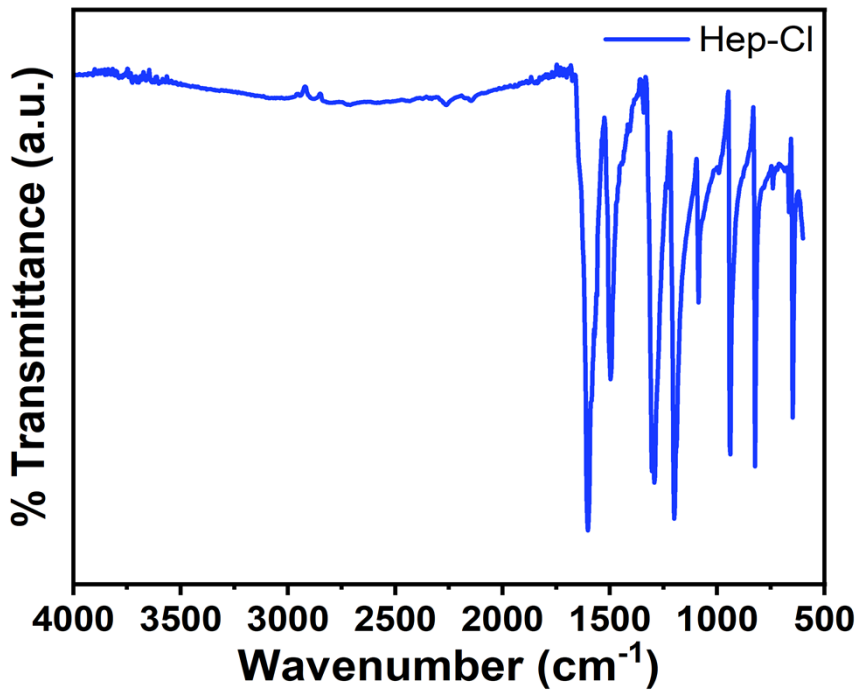

Fig. S2 FTIR spectrum of Heptazine Chloride.

Photocatalytic sulfide oxidation procedure:

A 10 mL round bottom flask equipped with a magnetic stir bar was charged with 0.1 mmol of sulfide, 10 mg of photocatalyst (HEP-FL or TZ-FL), and 3 mL solvent. The round bottom flask (RB) was closed using a rubber septum and the reaction mixture was purged with the oxygen gas for 10 min directly using an O_2 filled balloon with the help of a long needle. The pressure of the reaction system was equivalent to atmospheric pressure. Finally, the reaction mixture was stirred at room temperature under blue LED light irradiation (λ = 450 nm). After completion of the reaction, the mixture was centrifuged and the catalyst was recovered. The filtrate was extracted using ethyl acetate (3 x 2 mL) and after evaporation under reduced pressure, the product was characterized using NMR spectroscopy (using deuterated chloroform). The sulfide conversion was calculated based on the integration of methyl protons (adjacent to sulfur) in the reactant and products in the NMR spectra.

Recyclability test:

0.1 mmol of methyl phenyl sulfide, 3 mL H2O and 10 mg of photocatalyst (HEP-FL) were added into 10 mL round bottom flask equipped with a magnetic stir bar. The reaction was performed under oxygen atmosphere at room temperature under 20 W blue LED light irradiation for 1.3 h. After the reaction, reaction mixture was centrifuged to separate the catalyst. The aqueous phase was extracted with ethyl acetate (3 x 2 mL) and rota evaporated. This crude reaction mixture was subjected to NMR for characterization. The recovered catalyst was washed with methanol and then dried in the oven. This recovered catalyst was reused for the next catalytic cycle.

We agree that substrate compatibility is a critical factor. We have now expanded our discussion by including aliphatic sulfides as per the reviewer's suggestion. From the experimental results, we can conclude that HEP-FL is efficient in oxidation of broad range of sulfides including both aromatic and aliphatic sulfides.

General procedure for H_2O_2 detection by iodometric technique

After the completion of the photocatalytic sulfide oxidation reaction, the catalyst was separated by centrifugation, and filtrate was collected. To 100 μL of this filtrate, freshly prepared 450 μL of 0.4 M potassium iodide and 450 μL of 0.1 M potassium hydrogen phthalate aqueous solutions were added. This obtained solution was kept under the dark for 30 min and then analyzed by UV-vis spectroscopy. Under acidic conditions, H_2O_2 reacts with iodide (I^-) to produce iodide (I_3^-) which gives a strong absorbance at 350 nm.

Table S1. Performance of metal-based and metal-free photocatalysts employed for sulfide oxidation.

S. No.	Photocatalyst (Quantity)	Light Source	Solvent/Additive or Redox Mediator	Time (min)	Conv. (%)	Select. (%)	Ref.
			Metal-based photocatalysts				
1.	3%-C_{60}@PCN-222 (MOF) (15 mg)	LED lamp (50 mW/cm^2, λ > 400 nm)	CH_3OH	180	>99	100	1
2.	NNU-45 (MOF) (4 mg)	300 W Xe lamp (λ > 420 nm)	CH_3OH:$CHCl_3$ (1:4)/H_2O_2	240	99	95	2
3.	h-LZU1 (10 mg)	300 W Xe lamp (λ > 380 nm)	CH_3CN	1320	100	92.6	3
4.	DhaTph-Zn (10 mg)	300 W Xe lamp (λ > 400 nm)	CH_3CN	600	82	>99	4
5.	Zr_{12}-NBC (2 mol % based on photosensitizer)	24 W blue LED	CH_3OH	600	100	100	5
6.	2-AA-TiO_2 (40 mg)	Violet LEDs (410 nm, 3 W × 4)	CH_3OH/TEA	50	85	88	6
7.	4-NA-Cu_2O RDs (2.9 mg)	40 W blue LED	CH_3OH:H_2O (1:2)	720	98	96	7
8.	Zr_6-Irphen (4 mol %, based on Ir)	100 W blue LED (λ = 460 nm)	H_2O	360	98	100	8
9.	$Bi_4O_5Br_2$ (20 mg)	30 W blue LED	H_2O	360	99	98	9
10.	PW12-M@COFs (3 mg)	10 W 425 nm (LED)	CH_3CN	210	98	99	10
11.	$CdS_{0.109}$@Co-CP (9 mg)	blue LEDs	CH_3CN:H_2O (10:1)	480	95	100	11
12.	ARS-TiO_2 (9.6 mg)	300 W Xe lamp	CH_3OH	600	81	91	12
13.	Ir-SiW (0.25 μmol)	White LED lamp	CH_3OH	150	>99.5	-	13
14.	MOF-6 (0.84 μmol)	26 W fluorescent lamp	CH_3OH	1320	72	-	14
15.	Pt/$BiVO_4$ (50 mg)	Xe lamp (λ > 420 nm)	CH_3CN:H_2O (2:1)	300	70	98	15
			Metal-free photocatalysts				
16.	AQ-COF (10 mg)	300 W Xe lamp (λ = 400−780 nm)	CH_3CN	180	>99	97	16
17.	A-CTP-DPA (5 mg)	300 W Xe lamp (420 nm)	CH_3CN	240	99	93	17

18.	P-PDIP (5 mg)	visible light (420 < λ < 780 nm, 0.45 W/cm^2)	CH_3OH	180	>99	>99	18
19.	TPBTD-COF (5 mg)	Blue LED	CH_3OH/TEMPO	162	96	96	19
20.	PTBC-Por COF (10 mg)	150 W Xe lamp	CH_3CN: CH_3OH (12:5)	60	97	>99	20
21.	C-CMP (20 mg)	Visible light	CH_3CN	480	99	93	21
22.	CPTPA-COF (8 mg)	LED light	CH_3OH	180	100	100	22
23.	B-(Boc-CB)$_2$-BT (10 mg)	blue light LED lamp	CH_3CN	1440	99	95	23
24.	4% C_{60}/g-C_3N_4 (30 mg)	Xe lamp	CH_3OH	120	94	100	24
25.	TCPP-CMP (10 mg)	white LED (100 W)	CH_3CN:H_2O (1:1)	960	99	97	25
26.	**HEP-FL (10 mg)**	**20 W Blue LED (λ=450 nm)**	**H_2O**	**80**	**100**	**100**	**This work**

Note: In all the above reports, the results are mentioned based on the methyl phenyl sulfide as substrate.

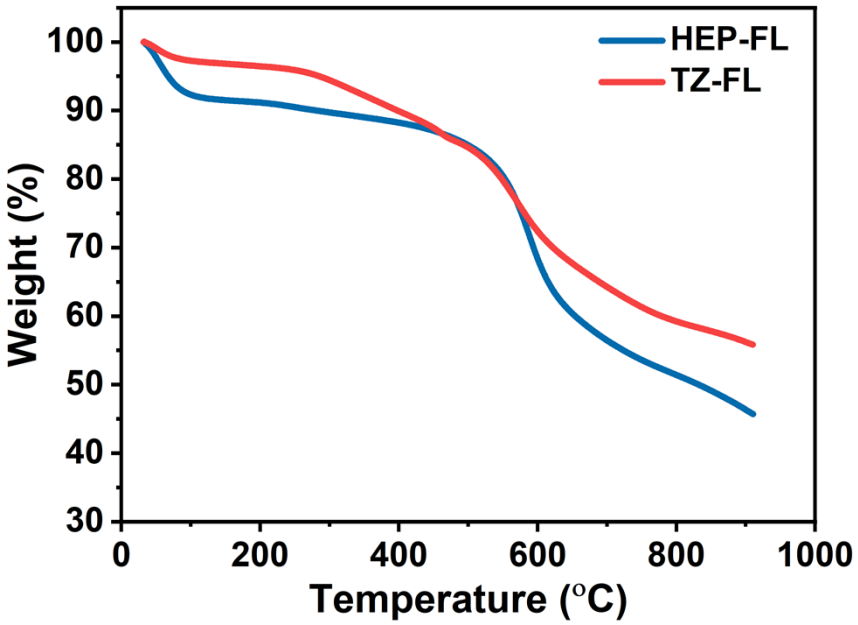

Fig. S3 TGA plot of HEP-FL and TZ-FL (under N_2 atmosphere).

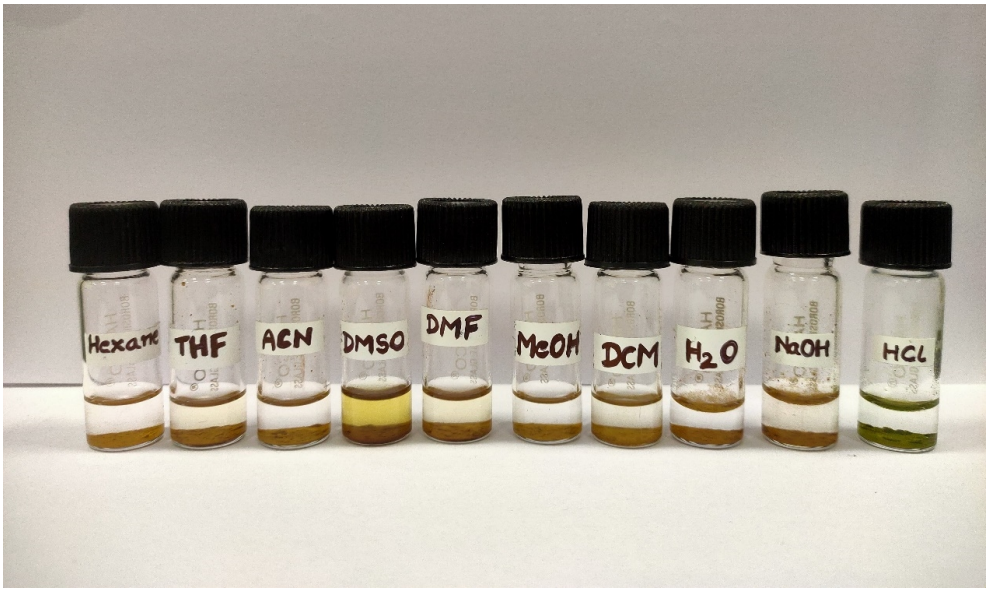

Fig. S4 HEP-FL immersed in various organic solvents, water, 6 M NaOH, and 6 M HCl for 3 days.

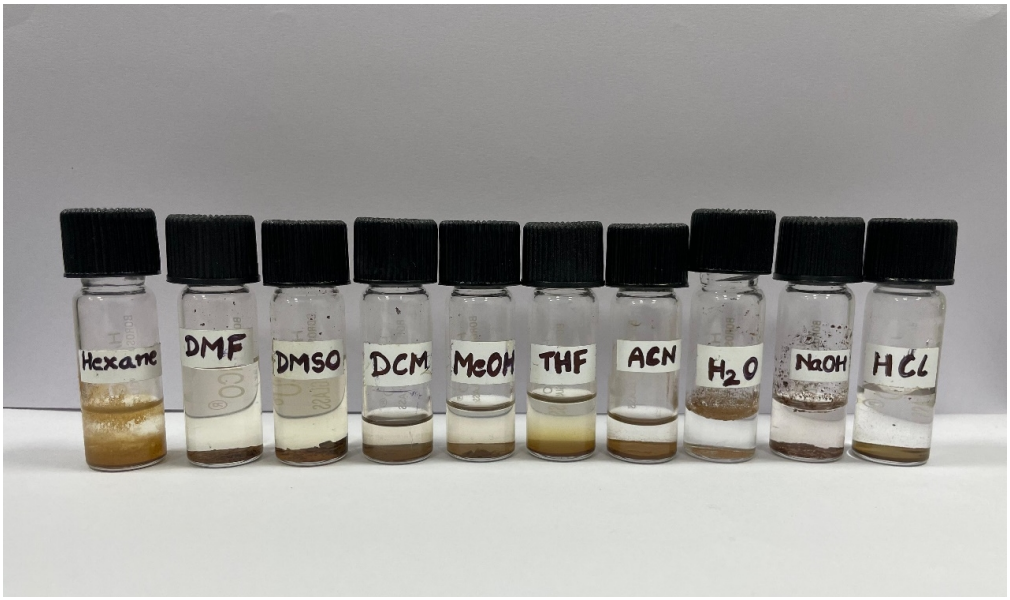

Fig. S5 TZ-FL immersed in various organic solvents, water, 6 M NaOH, and 6 M HCl for 3 days.

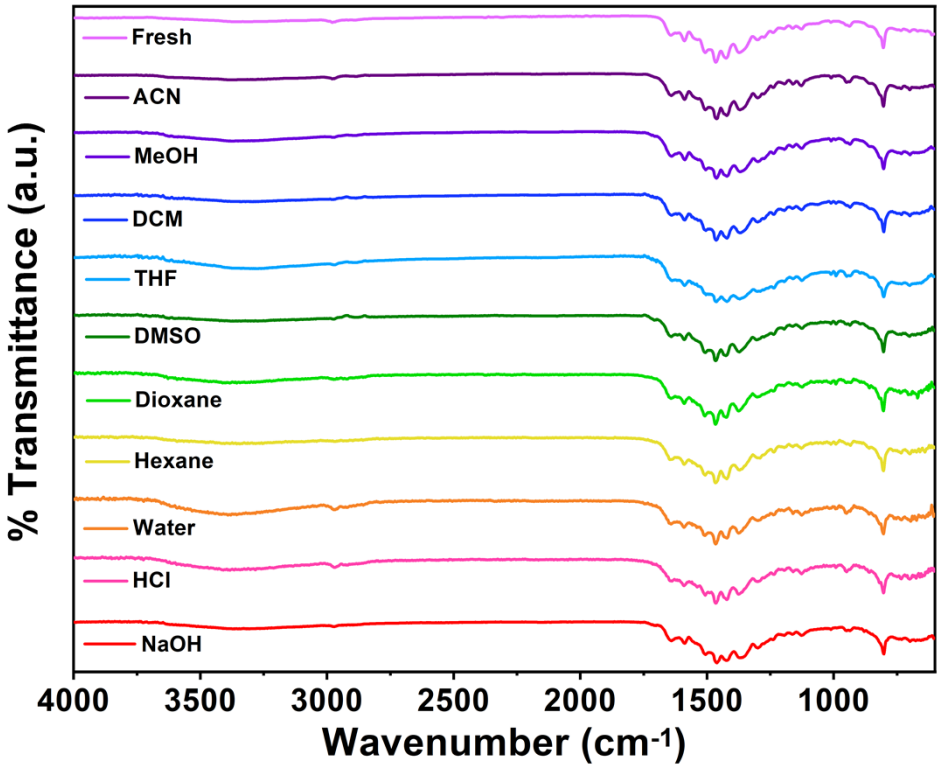

Fig. S6 Comparison of FTIR spectra of HEP-FL immersed into different solvents for 3 days.

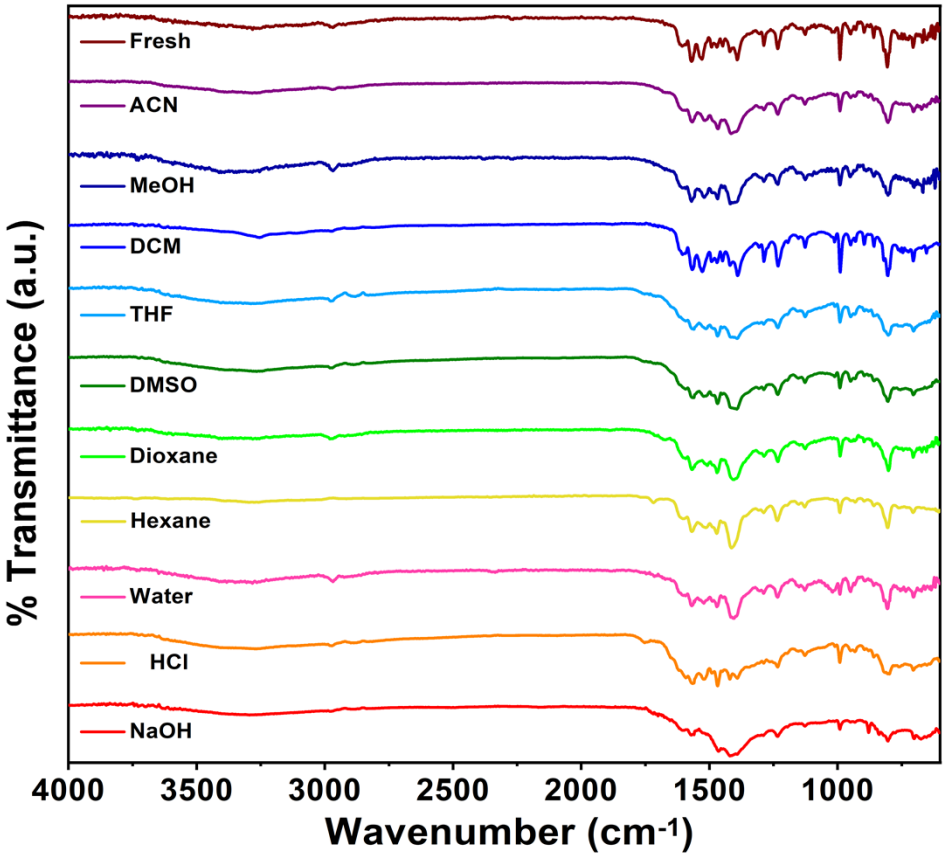

Fig. S7 Comparison of FTIR spectra of TZ-FL immersed into different solvents for 3 days.

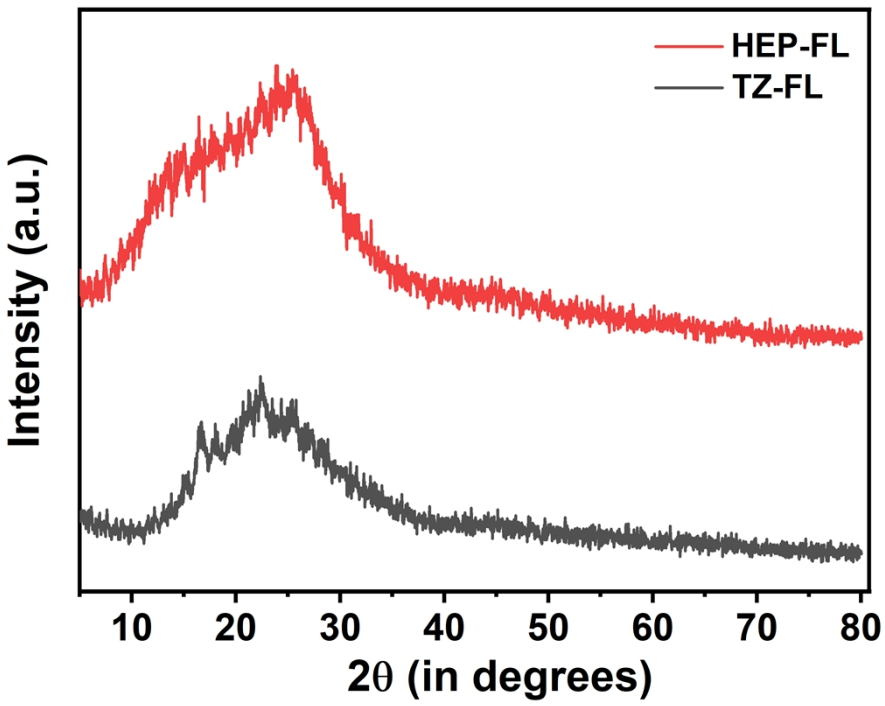

Fig. S8 PXRD pattern of polymeric networks HEP-FL and TZ-FL.

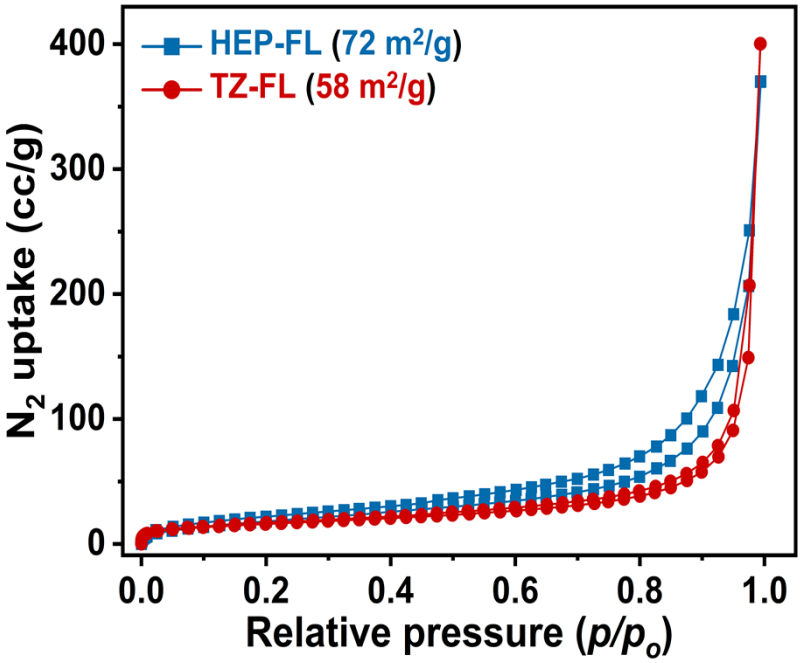

Fig. S9 N_2 physisorption isotherm of HEP-FL and TZ-FL.

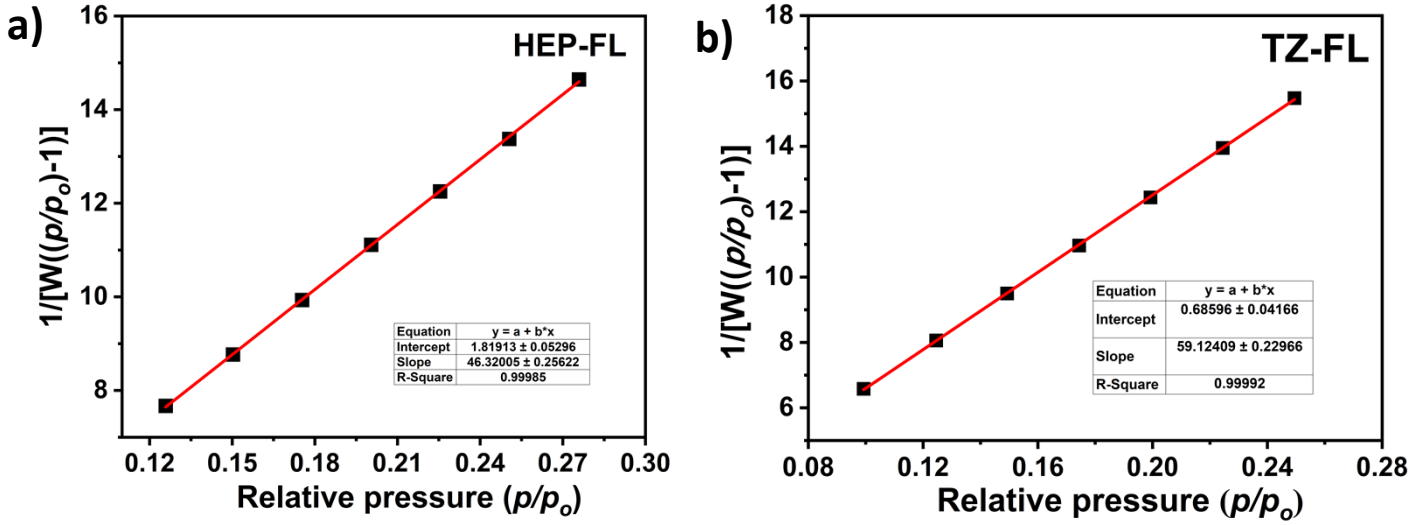

Fig. S10 Linear BET plot of (a) HEP-FL and (b) TZ-FL.

Green metrics parameters calculations:

Scientific scrutiny was applied to conduct green chemistry metrics analyses on the catalytic hydrogen transfer reaction involving carbonyl compounds, with the aim of scrutinizing both the environmental repercussions and the sustainability quotient of the reaction. Deliberate attention was directed towards an exhaustive examination of the pivotal parameters requisite for fostering a chemically green and sustainable reaction milieu.

Green chemistry metrics were applied to analyze the catalytic hydrogen transfer reaction of carbonyl compounds, with the objective of investigating its environmental impact and sustainability. A comprehensive examination of crucial parameters governing the green and sustainable nature of the reaction was undertaken.

1. Atom Economy (AE)

Atom economy is the measure of the number of atoms from the starting materials that are present in the useful products at the end of the chemical process. Good atom economy means most of the atoms of reactants are incorporated into final products and hence lesser problems of waste disposal. The ideal value of AE factor is 100%.

Atom economy serves as a quantitative measure of the efficiency with which atoms from the starting materials are incorporated into useful products during a chemical process. A high atom economy indicates that a significant proportion of the starting material is transformed into desired products, minimizing waste generation and disposal issues. The ideal value of the AE factor is 100%.

$$Atom\ Economy\ (AE) = \frac{Molecular\ weight\ of\ products}{\sum(Molecular\ weight\ of\ stochiometric\ reactants)} X\ 100$$

The atom economy for the model reaction was determined to be 100%, indicating that all atoms originating from the starting materials were incorporated within the useful products.

2. Process Mass Intensity (PMI)

Process Mass Intensity (PMI) serves as a benchmark for assessing the environmental sustainability of a process, concentrating on the total mass of materials utilized to generate a

specific mass of product. PMI accounts for all materials used within a chemical process, including reactants, reagents, solvents (with the exception of water), and catalysts.

For the model reaction, MI was calculated to be 1.35.

$$Process\ Mass\ Intensity\ (PMI) = \frac{Total\ mass\ in\ process\ (including\ catalyst)}{Mass\ of\ products}$$

3. Reaction Mass Efficiency (RME)

Reaction Mass Efficiency (RME) quantifies the effectiveness with which the mass of reactants is converted into the desired product, typically represented as a percentage. It takes into account both atom economy and chemical yield. RME measures the "greenness" of a chemical reaction. Its values range from 0-100%. Higher RME values of the reactions are considered better for a clean and green process.

RME value for the model reaction was calculated to be 73.68%.

$$Reaction\ Mass\ Efficiency\ (RME) = \frac{Mass\ of\ products}{\sum(Mass\ of\ stochiometric\ reactants)} X\ 100$$

4. Carbon Economy

Carbon economy accounts for the total amount of carbon in the product to the total amount of carbon present in the reactants. This metric involves the assessment of the environmental sustainability of synthesis through exclusive consideration of carbon balance.

The carbon economy (CE) for the model reaction was determined to be 100%, denoting the preservation of carbon content between the reactant and the product.

$$Carbon\ \ Economy\ (CE) = \frac{Total\ carbon\ in\ products}{Total\ carbon\ in\ reactants} X\ 100$$

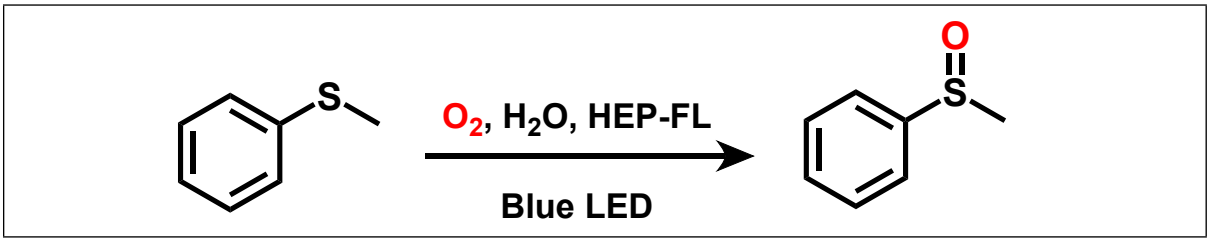

Table S2. Green metrics parameters for model sulfide oxidation reaction.

No.			
1.	Atom Efficiency (AE)	100%	100%
2.	Process Mass Intensity (PMI)	1	1.35
3.	Reaction Mass Efficiency (RME)	100%	73.68%
4.	Carbon Economy (CE)	100%	100%

S.No.	Catalyst	Reaction conditions (Solvent/ Time)	Conv% (Sel%)	Green metrics parameters			
				AE %	PMI	CE %	RME %
1.	**HEP-FL (this work)**	**3 mL H_2O/ 80 min**	**100 (100)**	**100**	**1.35**	**100**	**73.68**
2.	$Bi_4O_5Br_2$[9]	1 mL H_2O/ 360 min	99 (98)	100	1.76	100	56.66

Table S3. Comparison of green metrics parameters with reported photocatalysts for sulfide oxidation reaction.

3.	AQ-COF[16]	2 mL CH_3CN/ 180 min	99 (97)	100	1.89	100	52.63
4.	PTBC-Por COF[20]	6 mL CH_3CN, 2.5 mL CH_3OH/ 60 min	97 (99)	100	3.52	100	28.39
5.	Pt/$BiVO_4$[15]	1 mL CH_3CN, 0.5 mL H_2O/ 600 min	70 (98)	100	12.02	100	8.32
6.	CPTPA-COF[22]	2 mL CH_3CN/ 180 min	100 (100)	100	1.33	100	74.63
7.	4% C_{60}/g-CN[24]	5 mL CH_3OH/ 120 min	64 (100)	100	3.45	100	28.97

Conv= Conversion, Sel= Selectivity

AE= Atom Economy, PMI= Process Mass Intensity, CE= Carbon Economy, RME= Reaction Mass Efficiency

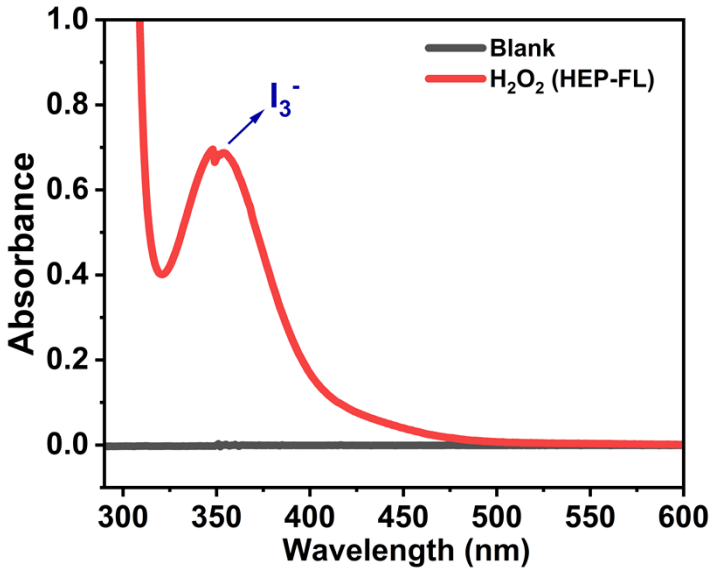

Fig. S11 H_2O_2 detection formed during photocatalytic sulfide oxidation reaction by iodometric technique using UV-vis spectroscopy.

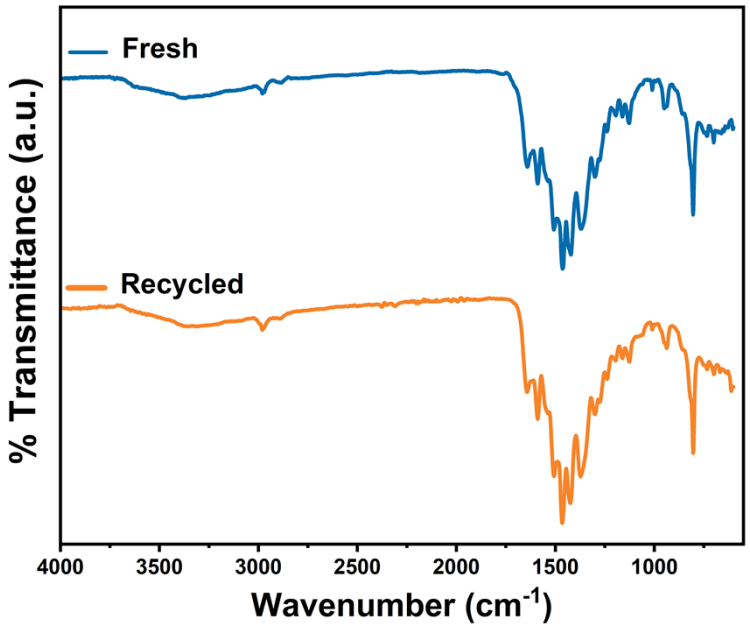

Fig. S12 Comparison of FTIR spectra before and after recyclability of HEP-FL.

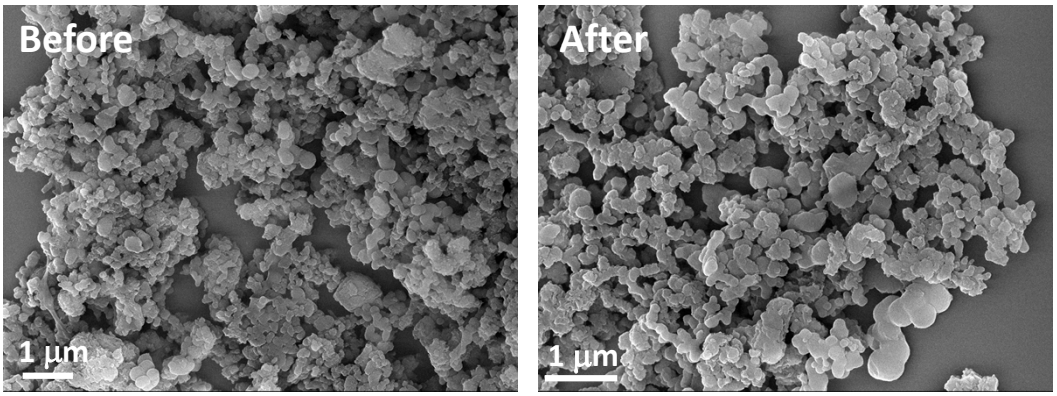

Fig. S13 FESEM images of HEP-FL before and after recyclability.

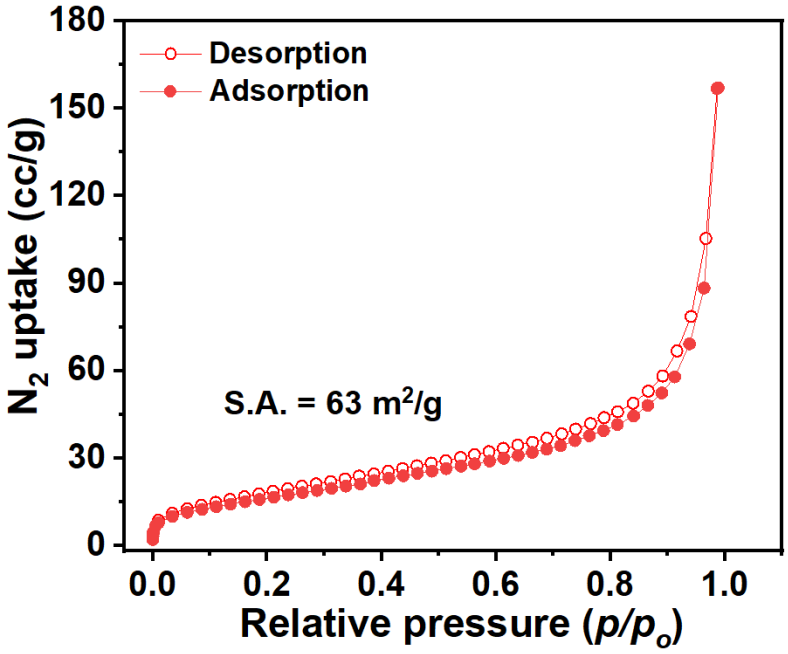

Fig. S14 N_2 physisorption isotherm of HEP-FL after recyclability.

NMR Data (chloroform-d)

Methyl phenyl sulfoxide

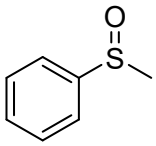

^{1}H NMR (400 MHz, $CDCl_3$) δ (ppm): 7.59-7.56 (dd, 2H), 7.48-7.41 (m, 2H), 2.65 (s, 3H)

^{13}C NMR (100 MHz, $CDCl_3$) δ (ppm): 145.58, 131.07, 129.36, 123.49, 43.98

4-Fluorophenyl methyl sulfoxide

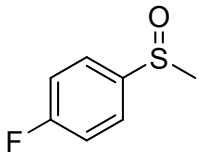

^{1}H NMR (400 MHz, $CDCl_3$) δ (ppm): 7.70-7.66 (m, 2H), 7.22-7.21 (m, 2H), 2.73 (s, 3H)

^{13}C NMR (100 MHz, $CDCl_3$) δ (ppm): 164.51, 141.20, 126.01, 116.58, 44.55

4-Chlorophenyl methyl sulfoxide

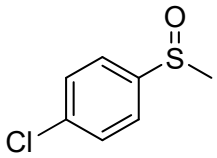

^{1}H NMR (400 MHz, $CDCl_3$) δ (ppm): 7.60-7.58 (m, 2H), 7.51-7.48 (m, 2H), 2.72 (s, 3H)

^{13}C NMR (100 MHz, $CDCl_3$) δ (ppm): 144.08, 13.08, 129.67, 125.05, 44.43

4-Bromophenyl methyl sulfoxide

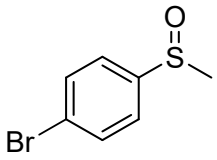

^{1}H NMR (400 MHz, $CDCl_3$) δ (ppm): 7.68-7.66 (d, 2H), 7.53-7.51 (d, 2H), 2.72 (s, 3H)

^{13}C NMR (100 MHz, $CDCl_3$) δ (ppm): 144.82, 132.58, 125.47, 125.16, 44.50

2-Chlorophenyl methyl sulfoxide

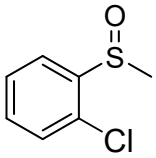

^{1}H NMR (400 MHz, $CDCl_3$) δ (ppm): 7.95-7.93 (dd, 1H), 7.55-7.51 (td, 1H), 7.46-7.42 (td, 1H), 7.39-7.37 (dd, 1H), 2.81 (s, 3H)

^{13}C NMR (100 MHz, $CDCl_3$) δ (ppm): 143.42, 132.01, 129.74, 128.13, 125.20, 41.57

2-Bromophenyl methyl sulfoxide

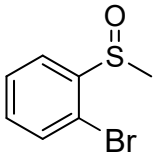

^{1}H NMR (400 MHz, $CDCl_3$) δ (ppm): 7.92-7.91 (dd, 1H), 7.57-7.51 (m, 2H), 7.37-7.33 (m, 2H), 2.79 (s, 3H)

^{13}C NMR (100 MHz, $CDCl_3$) δ (ppm): 145.12, 132.82, 132.25, 128.64, 125.53, 118.29, 41.78

4-Methylphenyl methyl sulfoxide

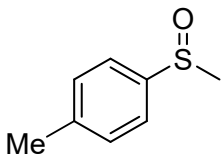

^{1}H NMR (400 MHz, $CDCl_3$) δ (ppm): 7.51-7.49 (d, 2H), 7.30-7.28 (d, 2H), 2.66 (s, 3H), 2.37 (s, 3H)

^{13}C NMR (100 MHz, $CDCl_3$) δ (ppm): 142.38, 141.53, 130.04, 123.53, 43.99, 21.43

4-Methoxyphenyl methyl sulfoxide

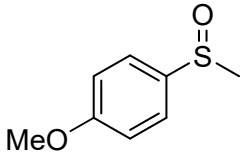

^{1}H NMR (400 MHz, $CDCl_3$) δ (ppm): 7.54-7.51 (d, 2H), 6.97-6.95 (d, 2H), 3.79 (s, 3H), 2.63 (s, 3H)

^{13}C NMR (100 MHz, $CDCl_3$) δ (ppm): 161.95, 136.33, 125.49, 114.83, 55.27, 43.71

4-Nitrophenyl methyl sulfoxide

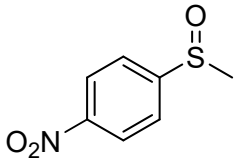

^{1}H NMR (400 MHz, $CDCl_3$) δ (ppm): 8.41-8.39 (d, 2H), 7.85-7.83 (d, 2H), 2.80 (s, 3H)

^{13}C NMR (100 MHz, $CDCl_3$) δ (ppm): 153.27, 149.53, 124.68, 124.66, 43.89

4-(methylthio) benzaldehyde

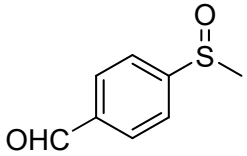

^{1}H NMR (400 MHz, $CDCl_3$) δ (ppm): 10.10 (s, 3H), 8.08-8.06 (d, 2H), 7.87-7.85 (d, 2H), 2.84 (s, 3H)

^{13}C NMR (100 MHz, $CDCl_3$) δ (ppm): 191.39, 152.18, 138.17, 130.34, 124.18, 43.52

Tetramethylene sulfoxide

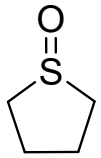

^{1}H NMR (400 MHz, $CDCl_3$) δ (ppm): 2.92-2.83 (m, 4H), 2.49-2.39 (m, 2H), 2.09-1.99 (m, 2H)

^{13}C NMR (100 MHz, $CDCl_3$) δ (ppm): 54.38, 25.34

Dibutyl sulfoxide

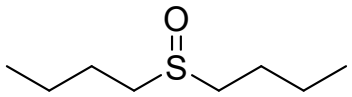

^{1}H NMR (400 MHz, $CDCl_3$) δ (ppm): 2.73-2.59 (m, 2H), 1.79-1.70 (m, 2H), 1.57-1.41 (m, 2H), 0.99-0.94 (m, 3H)

^{13}C NMR (100 MHz, $CDCl_3$) δ (ppm): 52.09, 24.55, 22.01, 13.63

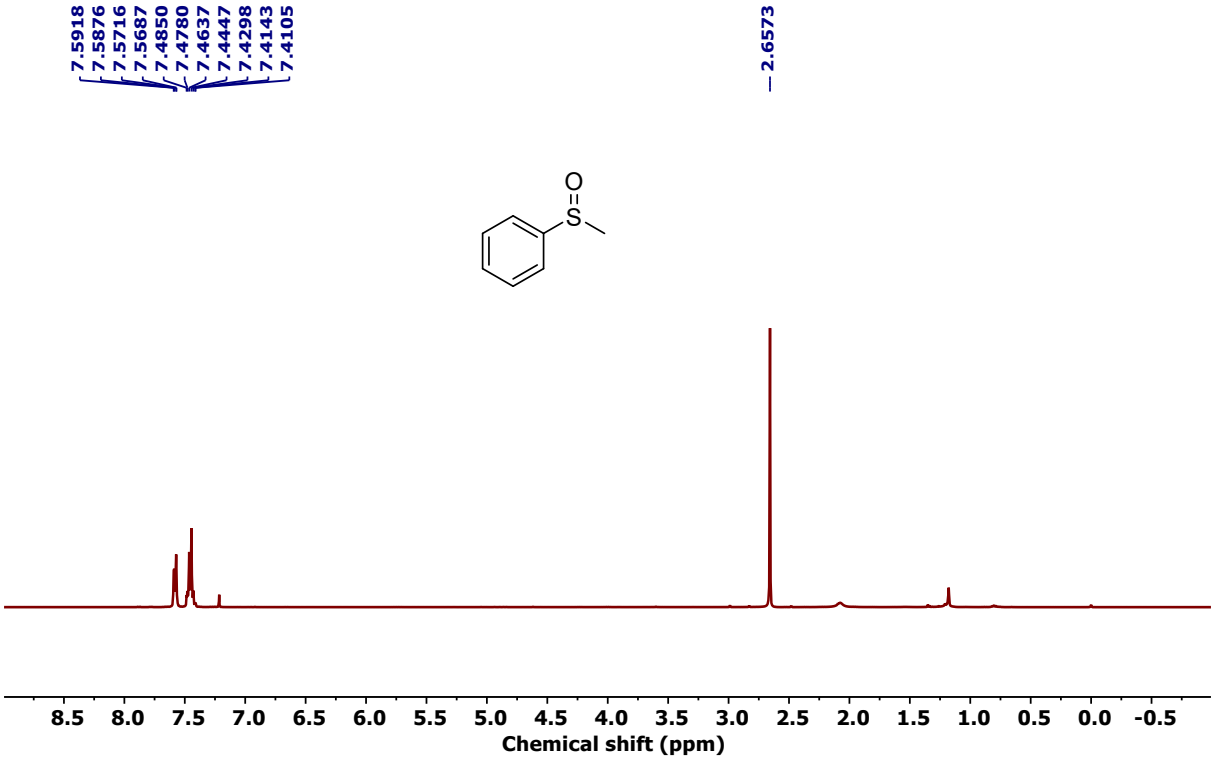

Fig. S15 ^{1}H NMR of methyl phenyl sulfoxide ($CDCl_3$, r.t.)

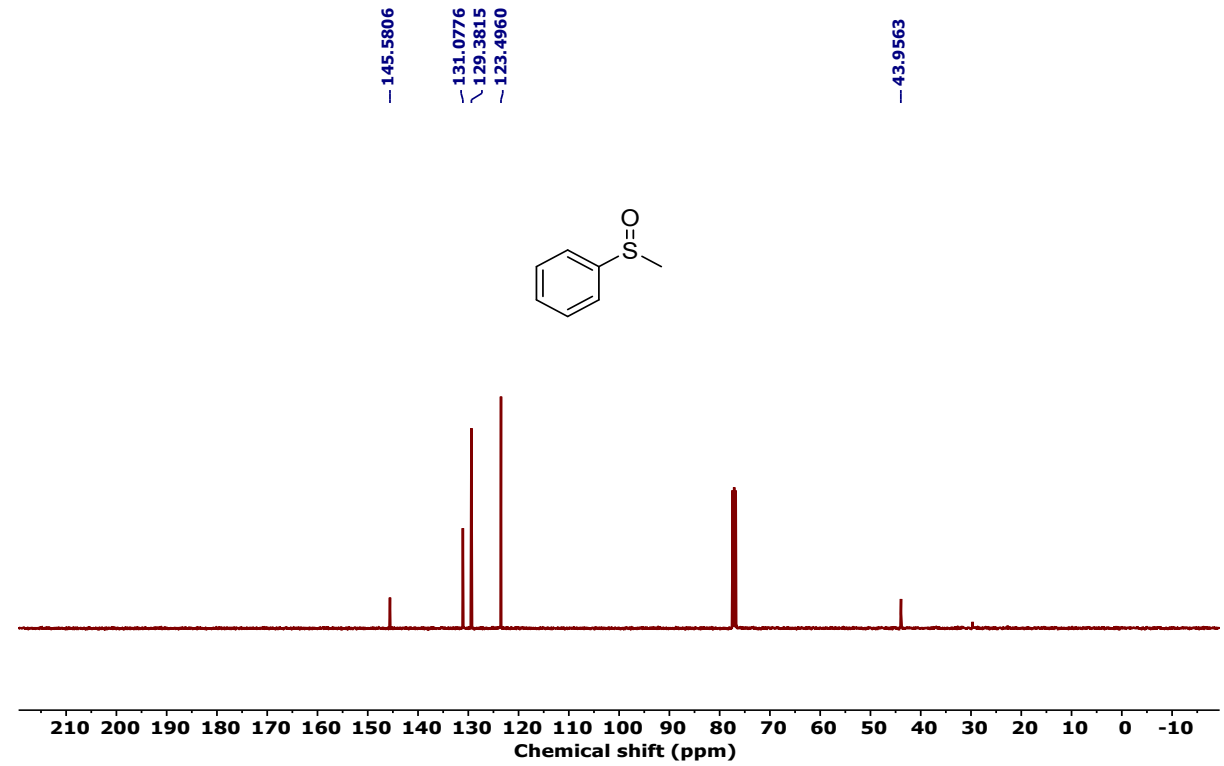

Fig. S16 ^{13}C NMR of methyl phenyl sulfoxide ($CDCl_3$, r.t.)

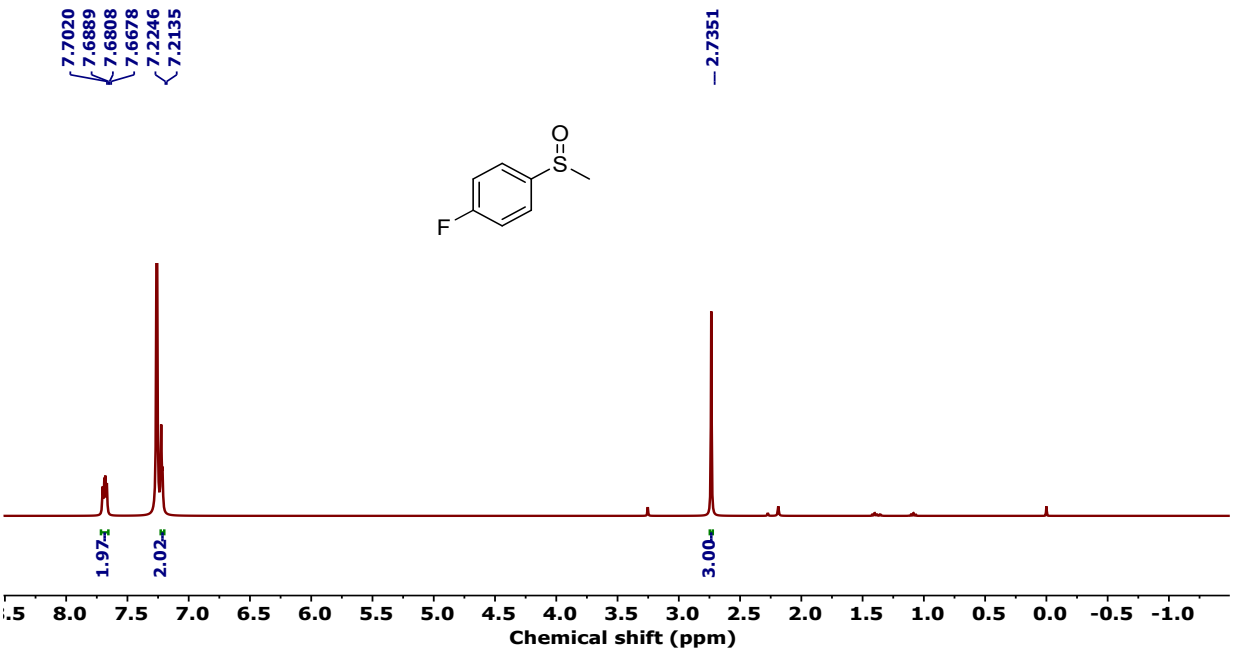

Fig. S17 ^{1}H NMR of 4-Fluorophenyl methyl sulfoxide ($CDCl_3$, r.t.)

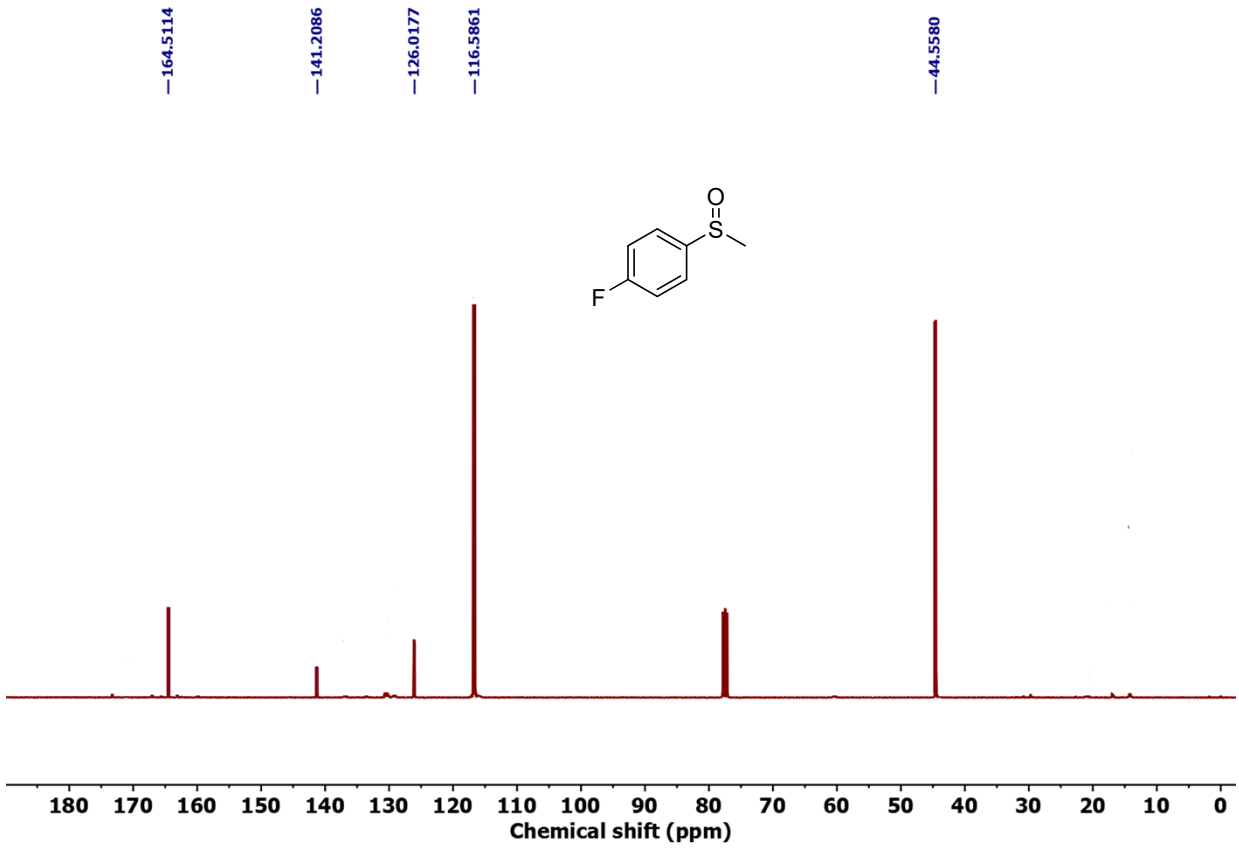

Fig. S18 ^{13}C NMR of 4-Fluorophenyl methyl sulfoxide ($CDCl_3$, r.t.)

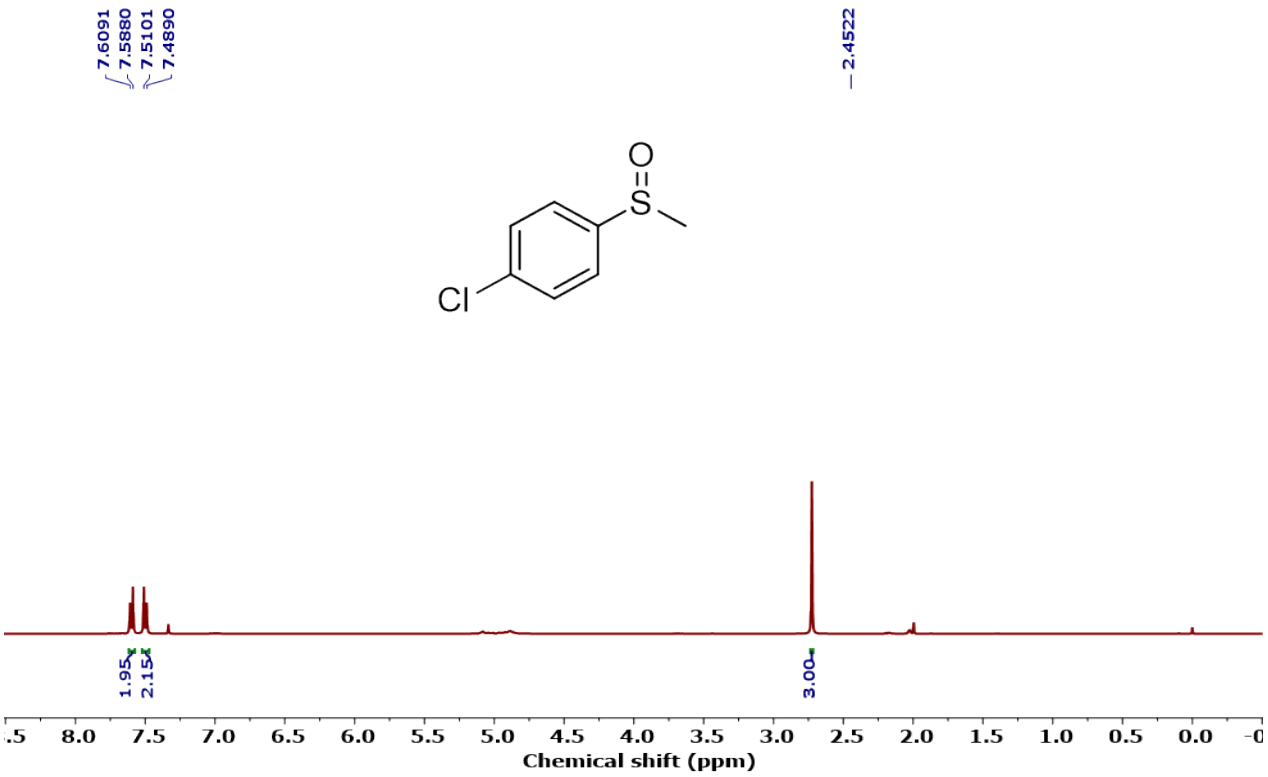

Fig. S19 ^{1}H NMR of 4-Chlorophenyl methyl sulfoxide ($CDCl_3$, r.t.)

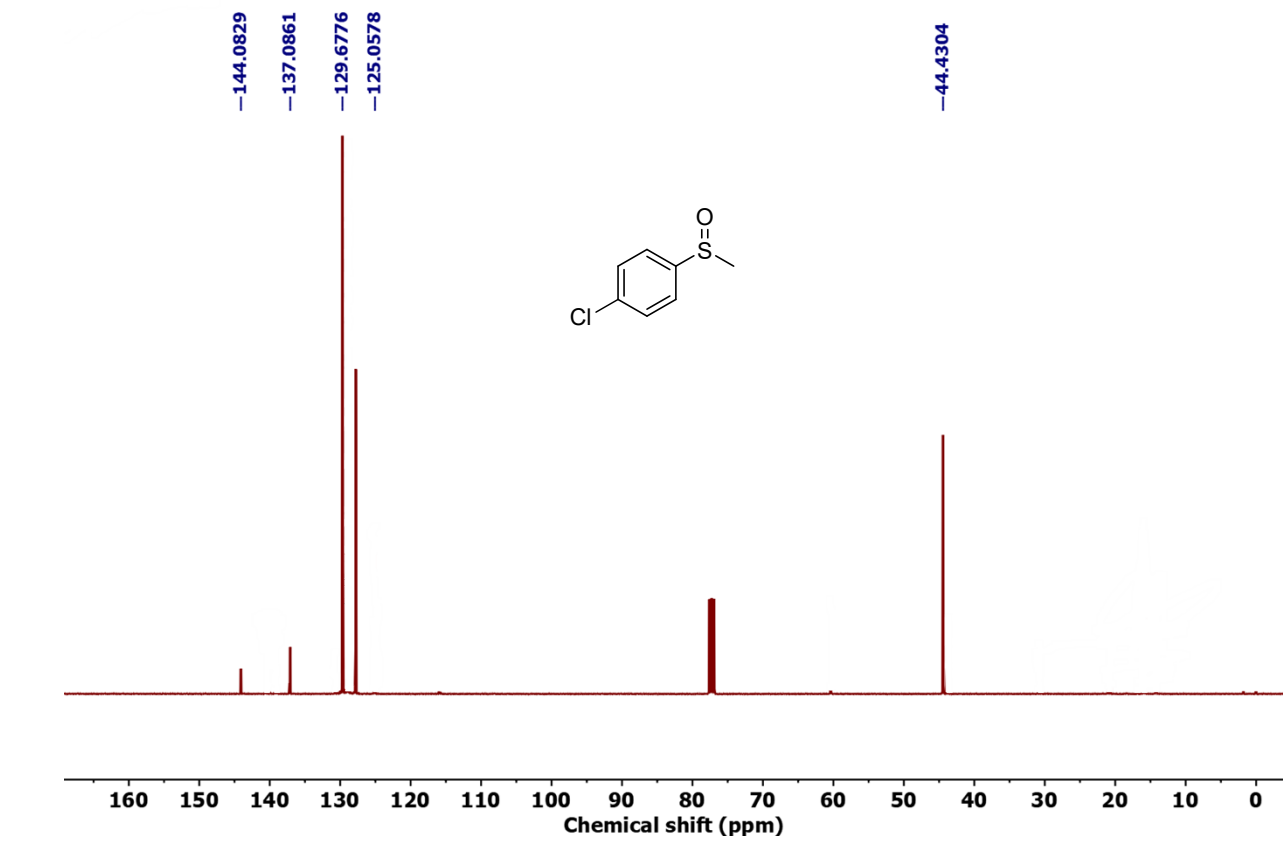

Fig. S20 ^{13}C NMR of 4-Chlorophenyl methyl sulfoxide ($CDCl_3$, r.t.)

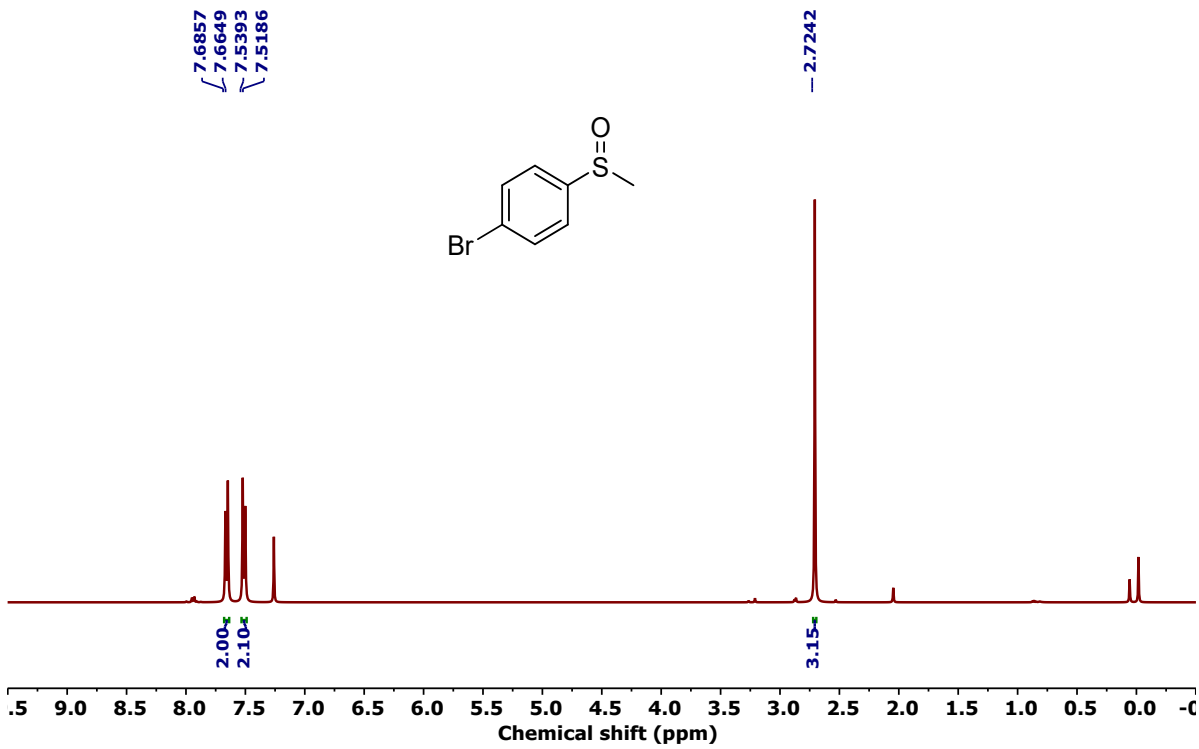

Fig. S21 ^{1}H NMR of 4-Bromophenyl methyl sulfoxide ($CDCl_3$, r.t.)

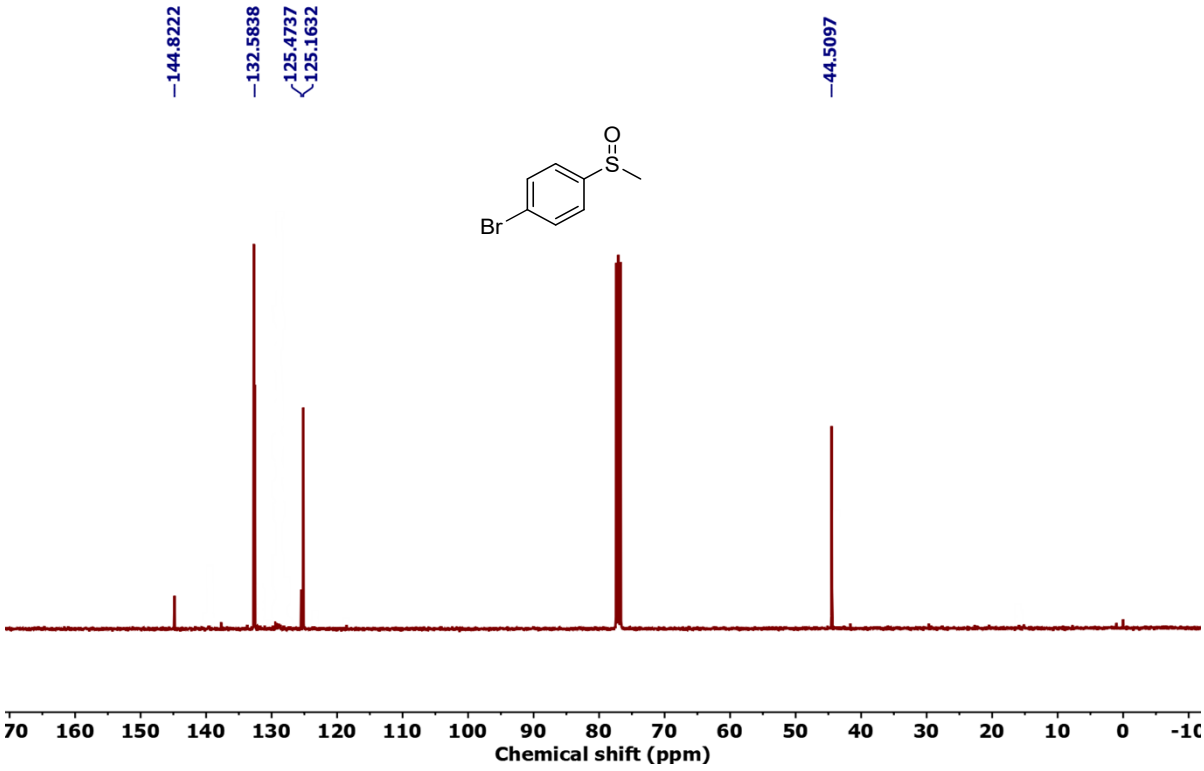

Fig. S22 ^{1}H NMR of 4-Bromophenyl methyl sulfoxide ($CDCl_3$, r.t.)

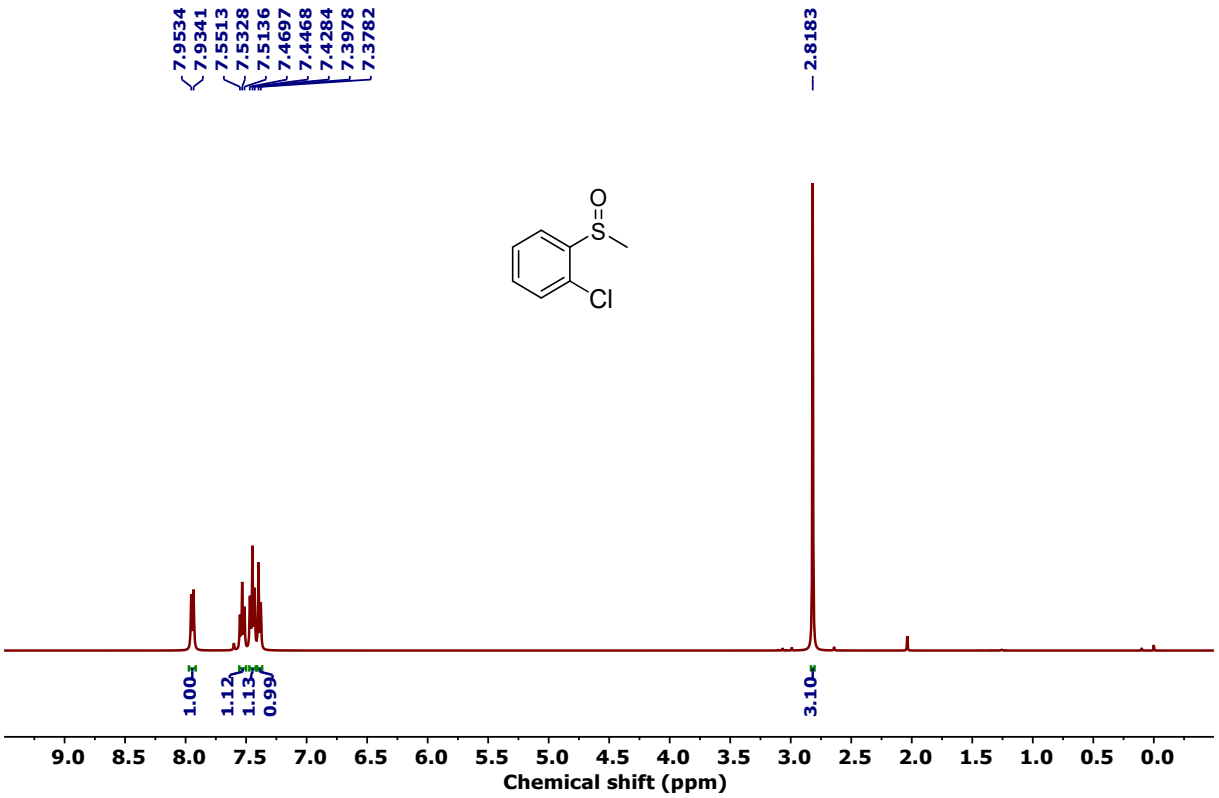

Fig. S23 ^{1}H NMR of 2-Chlorophenyl methyl sulfoxide ($CDCl_3$, r.t.)

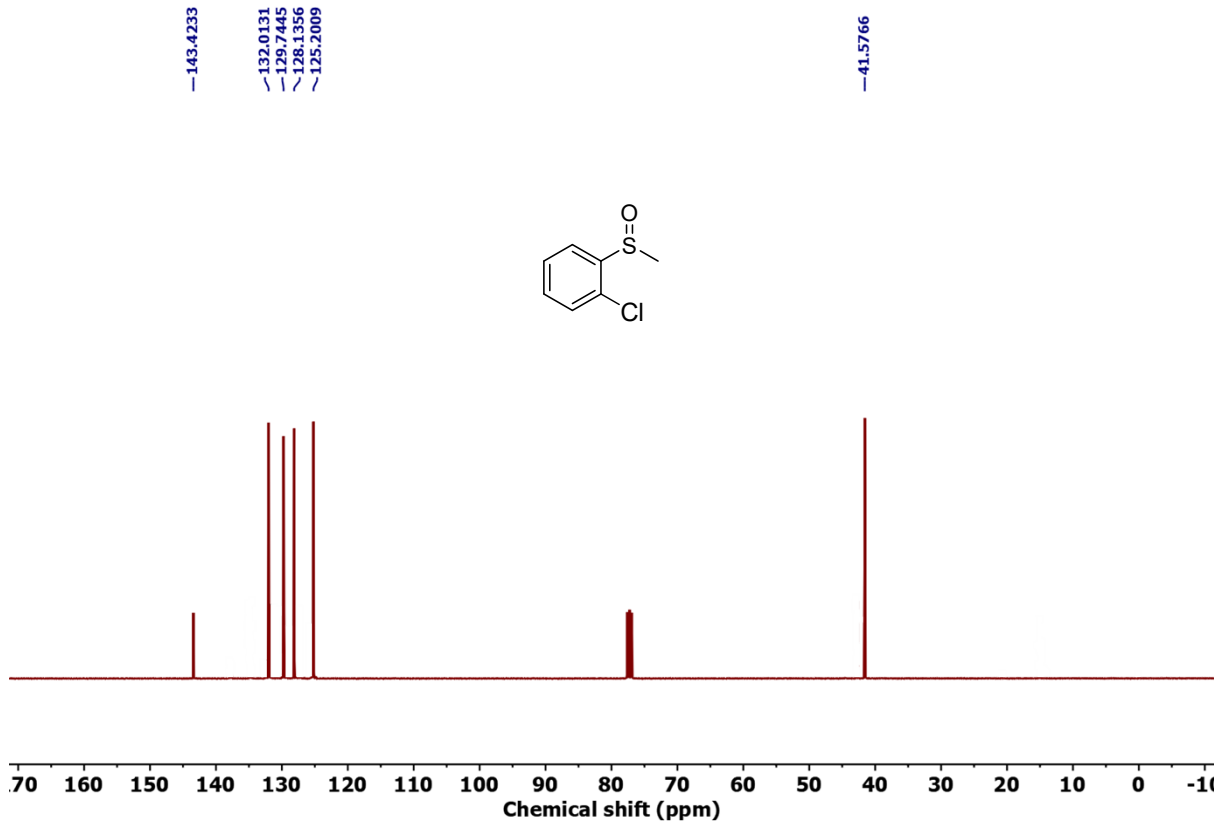

Fig. S24 ^{13}C NMR of 2-Chlorophenyl methyl sulfoxide ($CDCl_3$, r.t.)

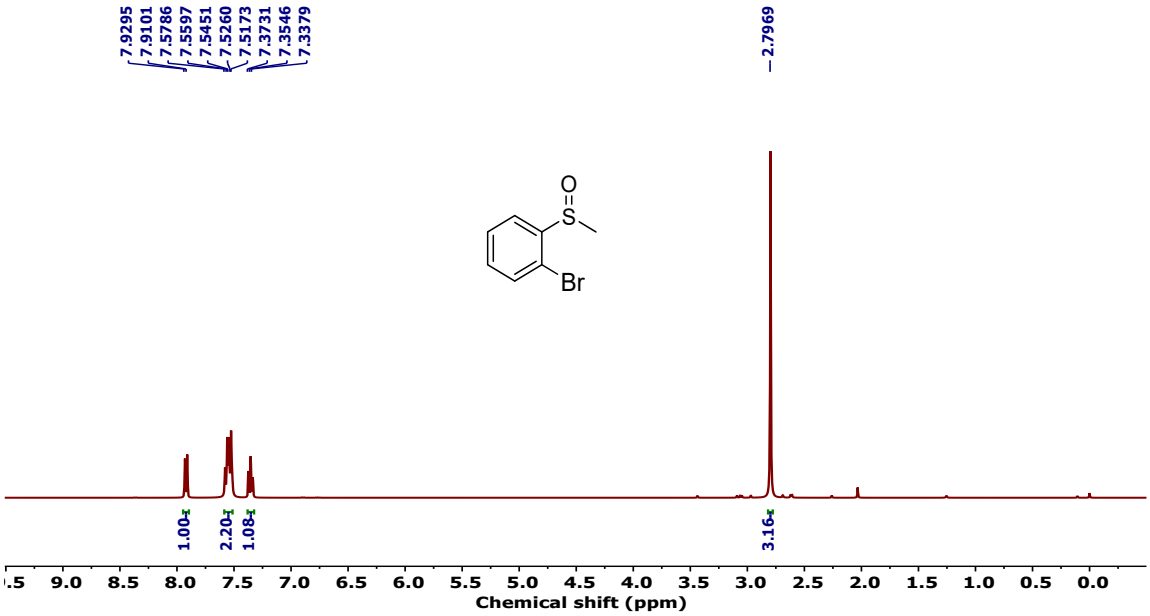

Fig. S25 ^{1}H NMR of 2-Bromophenyl methyl sulfoxide ($CDCl_3$, r.t.)

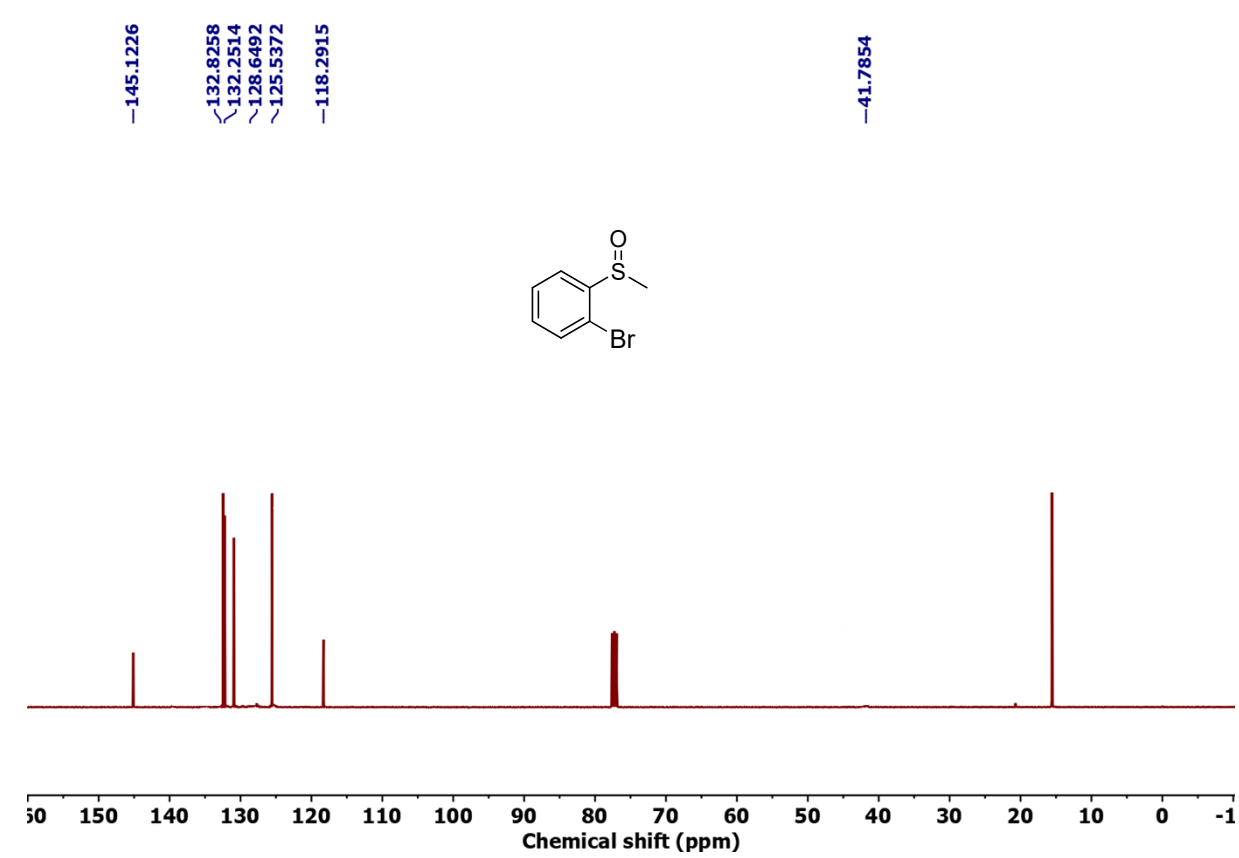

Fig. S26 ^{13}C NMR of 2-Bromophenyl methyl sulfoxide ($CDCl_3$, r.t.)

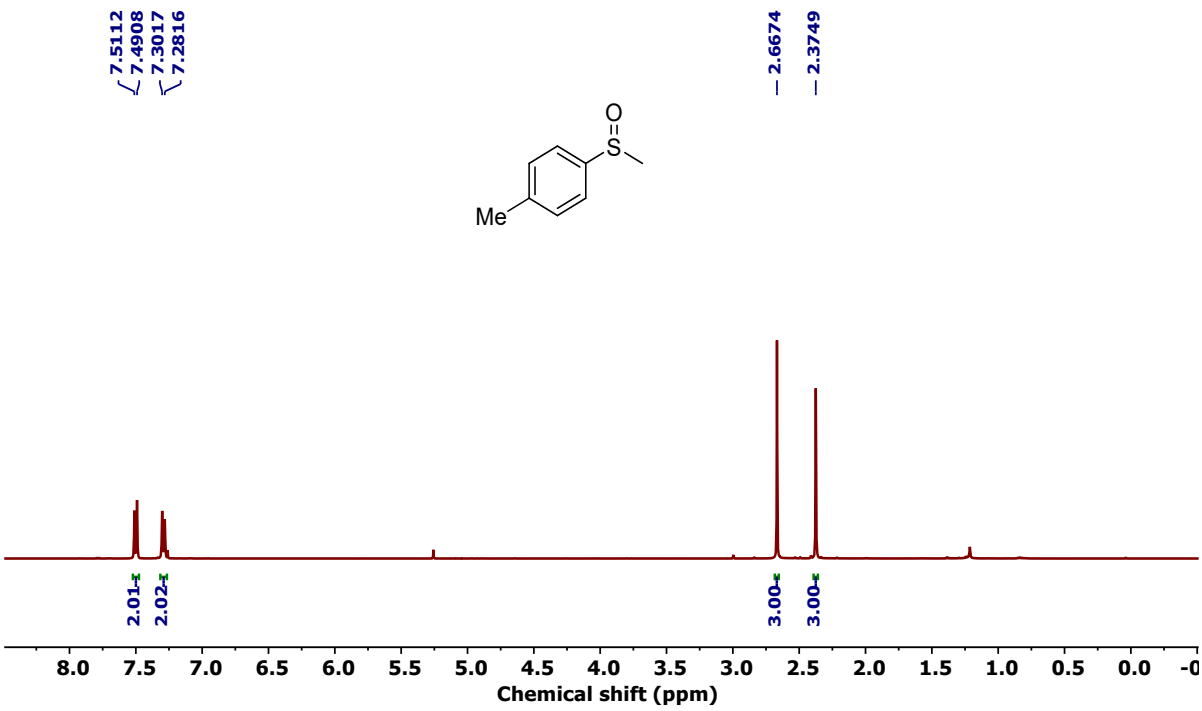

Fig. S27 ^{1}H NMR of 4-Methylphenyl methyl sulfoxide ($CDCl_3$, r.t.)

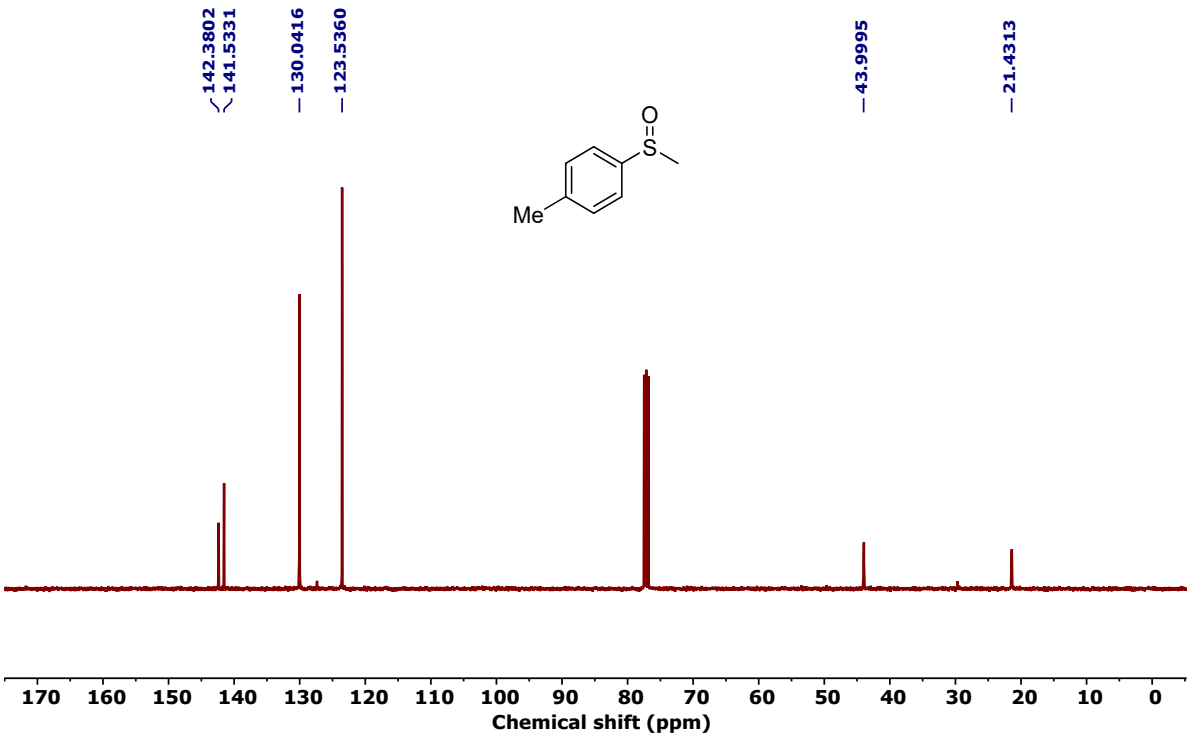

Fig. S28 ^{13}C NMR of 4-Methylphenyl methyl sulfoxide ($CDCl_3$, r.t.)

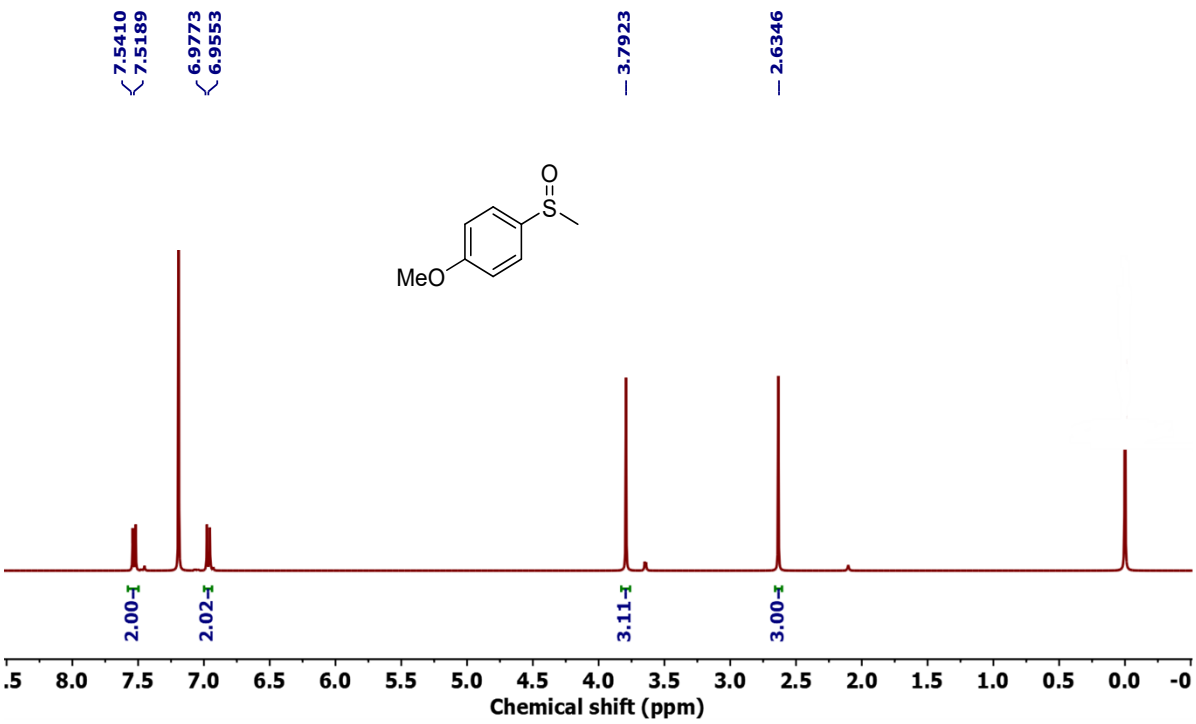

Fig. S29 ^{1}H NMR of 4-Methoxylphenyl methyl sulfoxide ($CDCl_3$, r.t.)

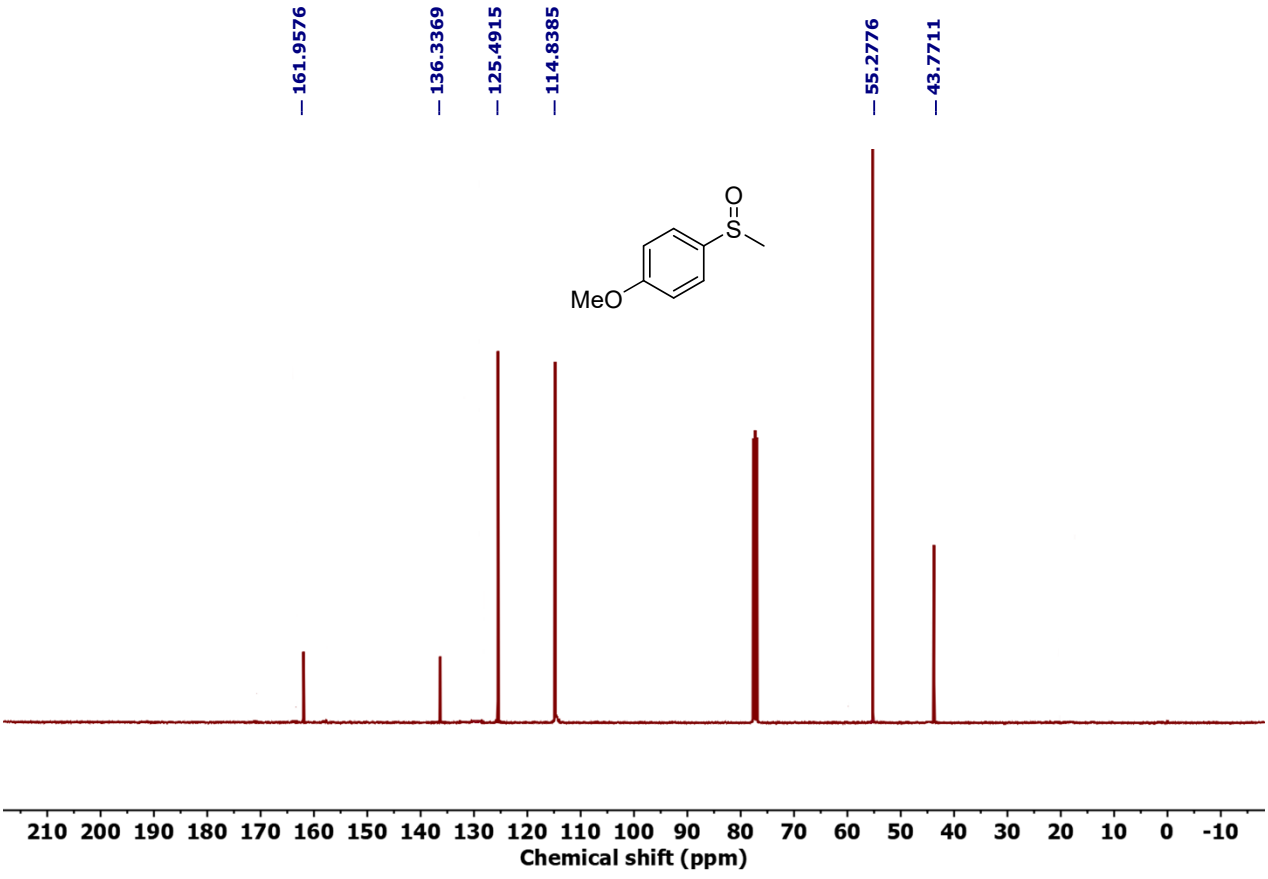

Fig. S30 ^{13}C NMR of 4-Methoxylphenyl methyl sulfoxide ($CDCl_3$, r.t.)

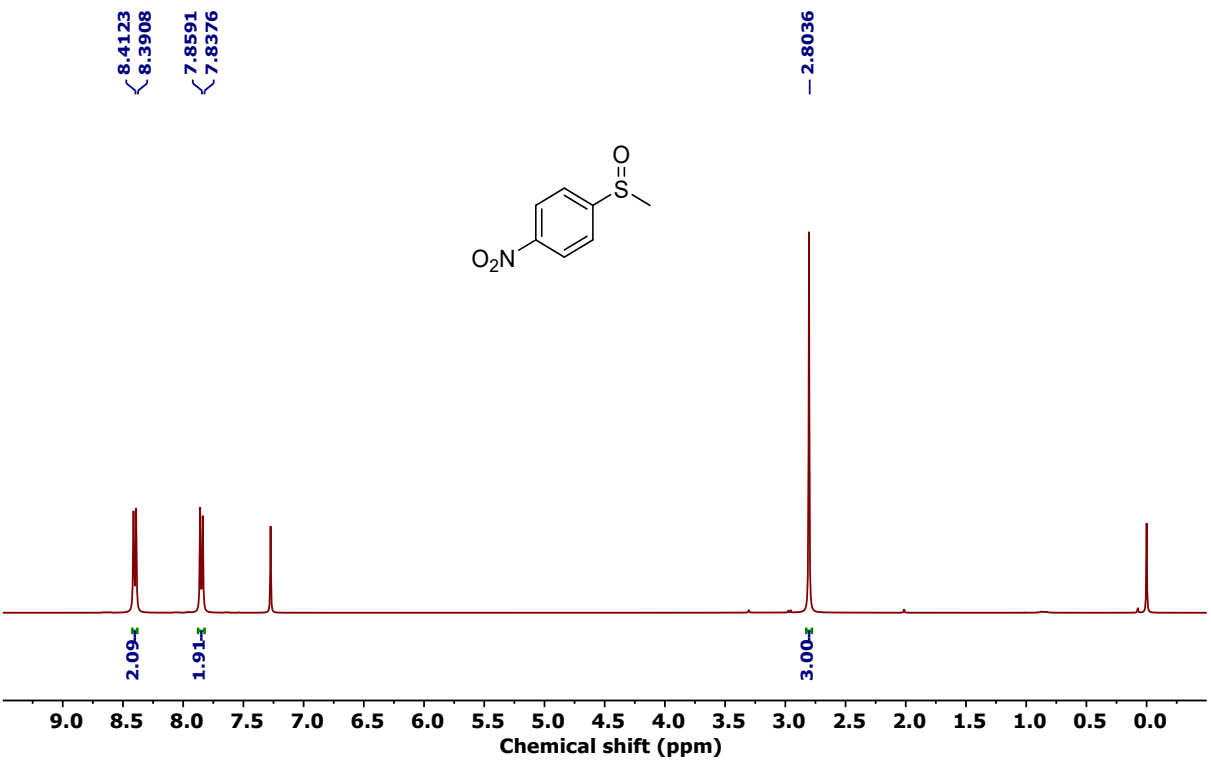

Fig. S31 ^{1}H NMR of 4-Nitrophenyl methyl sulfoxide ($CDCl_3$, r.t.)

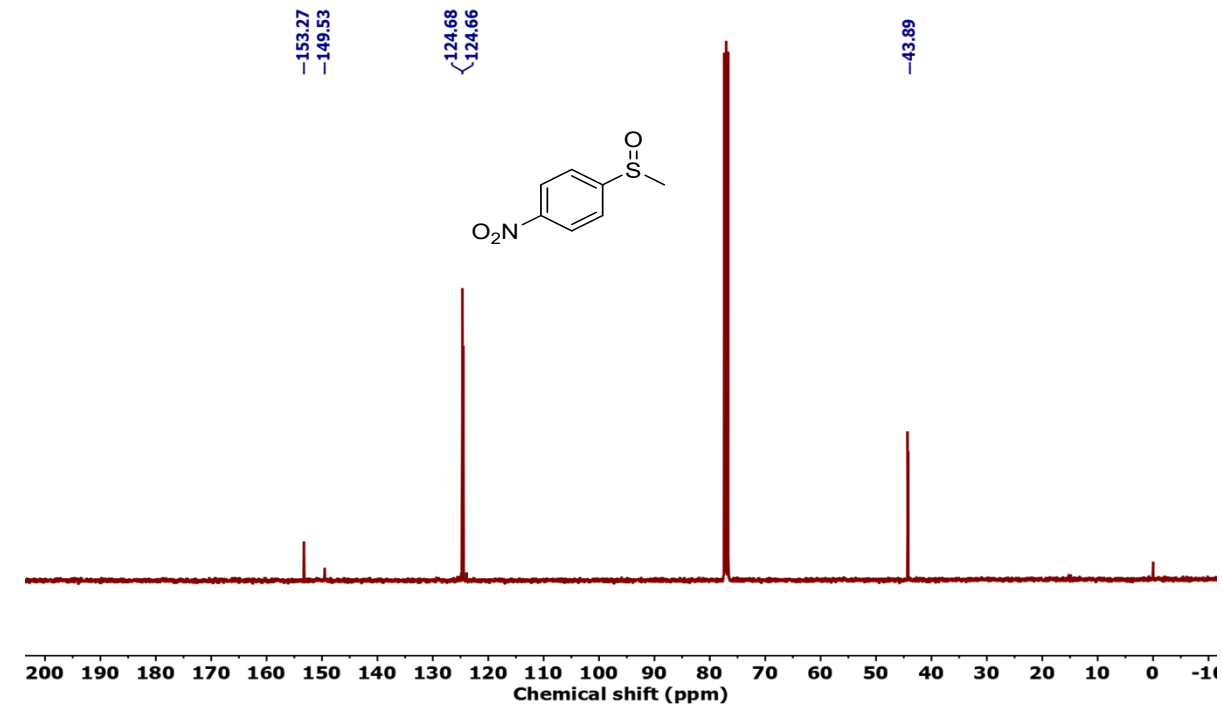

Fig. S32 ^{13}C NMR of 4-Nitrophenyl methyl sulfoxide ($CDCl_3$, r.t.)

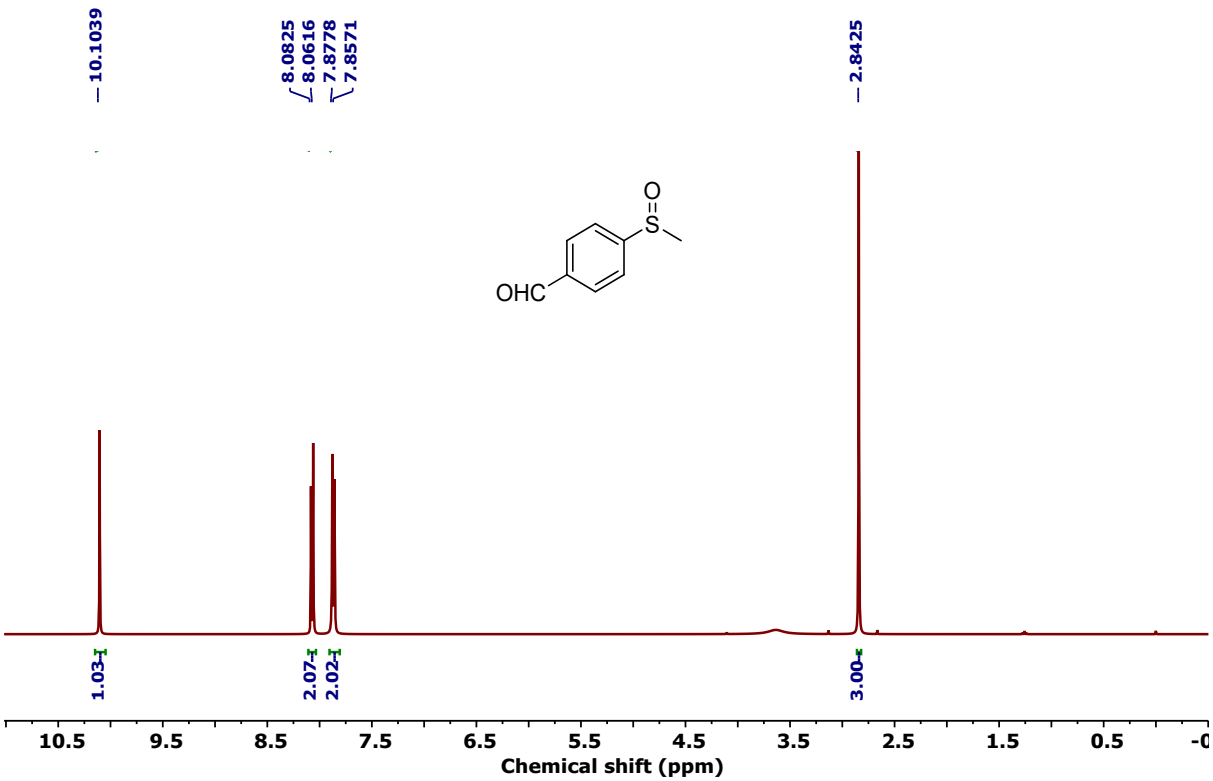

Fig. S33 ^{1}H NMR of 4-(methylthio) benzaldehyde ($CDCl_3$, r.t.)

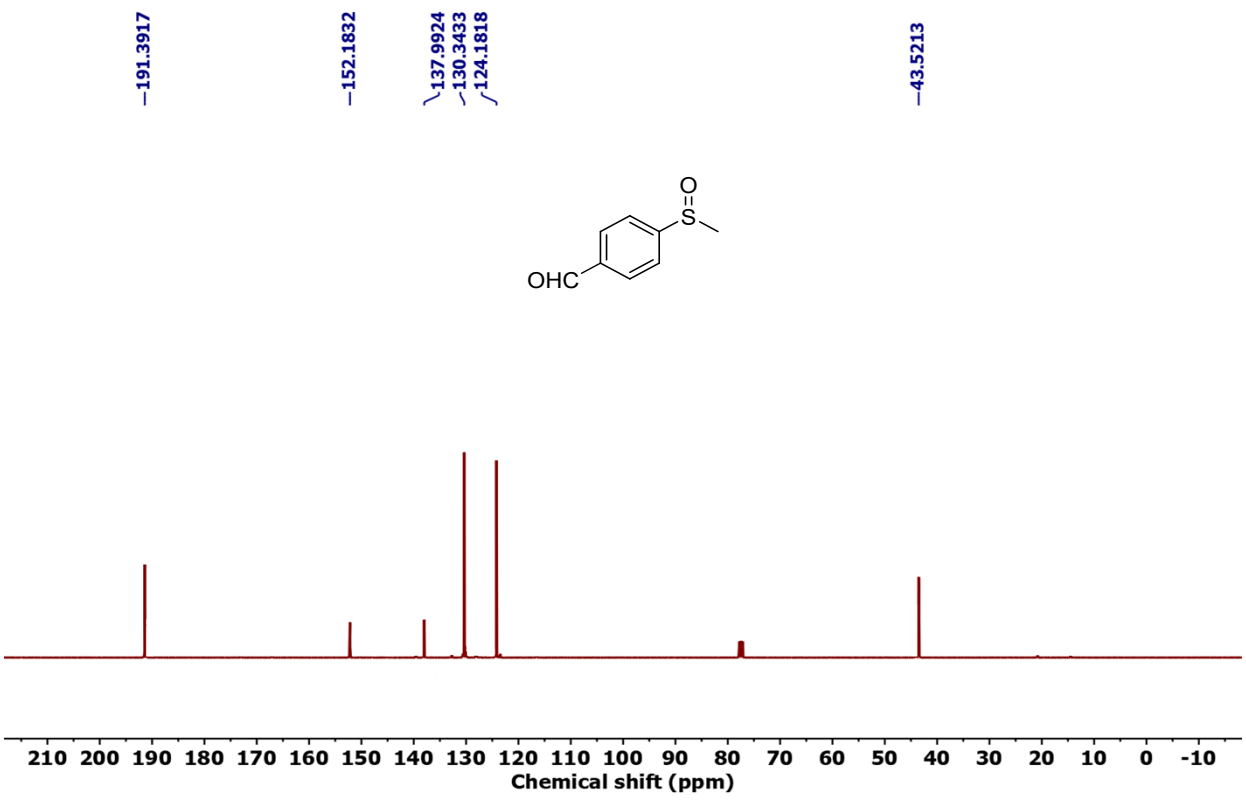

Fig. S34 ^{13}C NMR of 4-(methylthio) benzaldehyde ($CDCl_3$, r.t.)

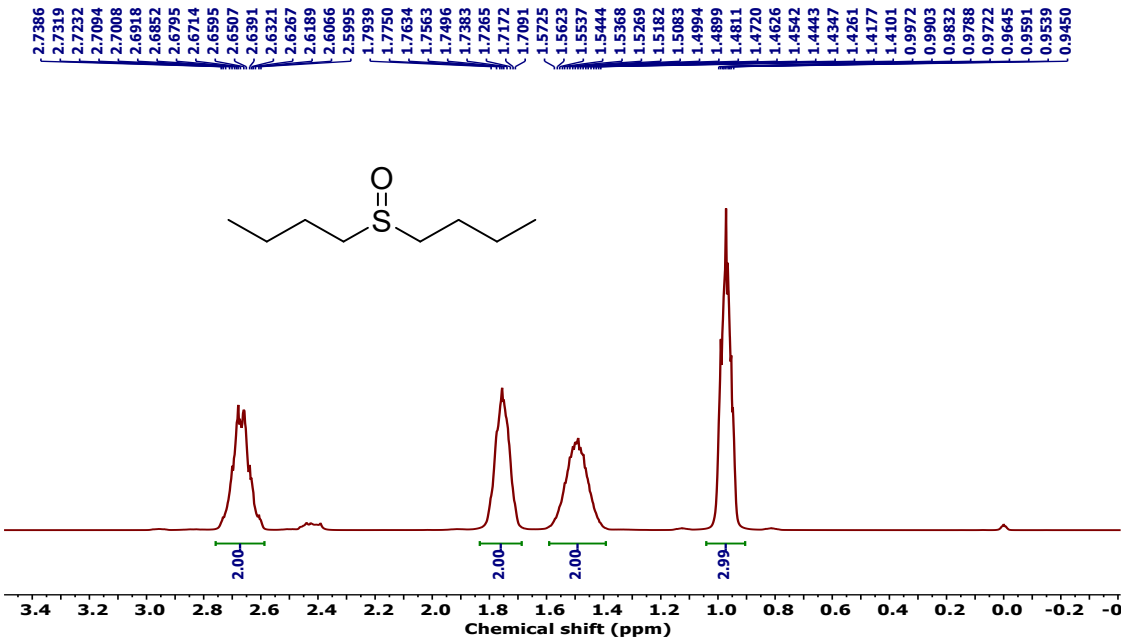

Fig. S35 ^{1}H NMR of Dibutyl sulfoxide ($CDCl_3$, r.t.)

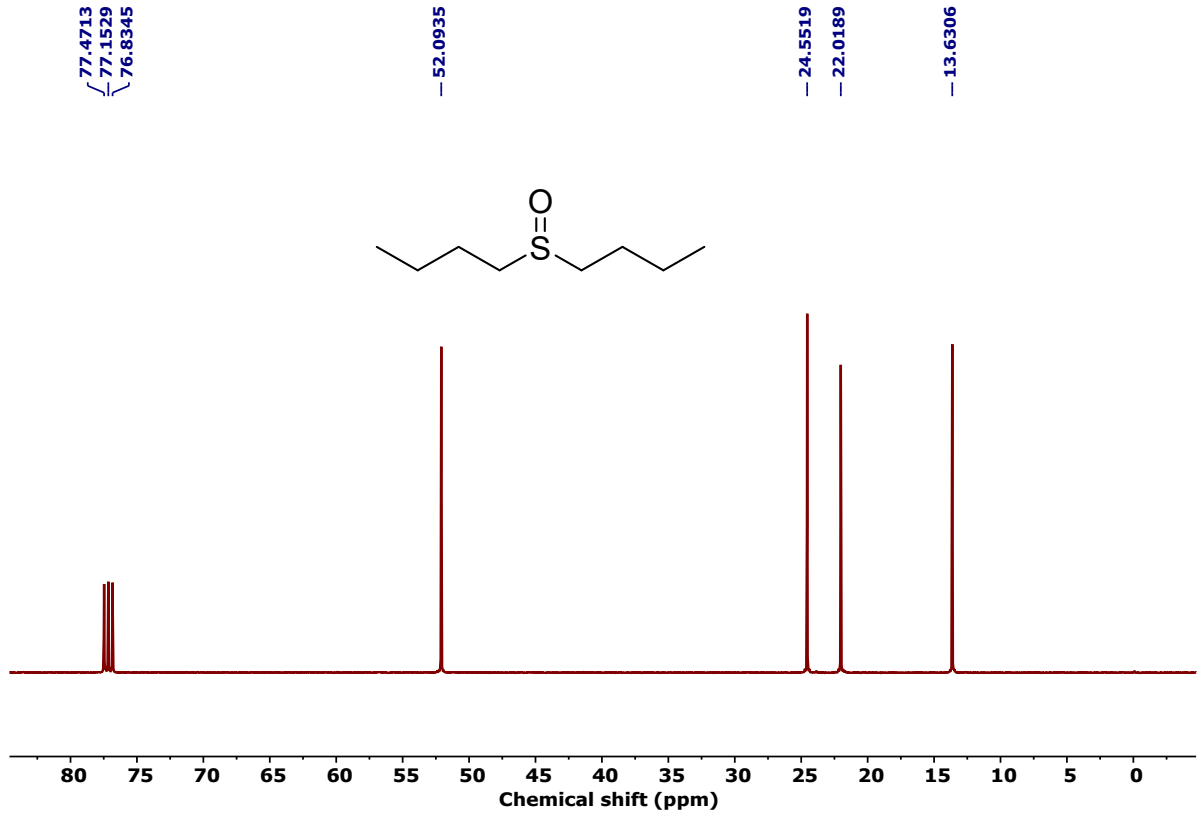

Fig. S36 ^{13}C NMR of Dibutyl sulfoxide ($CDCl_3$, r.t.)

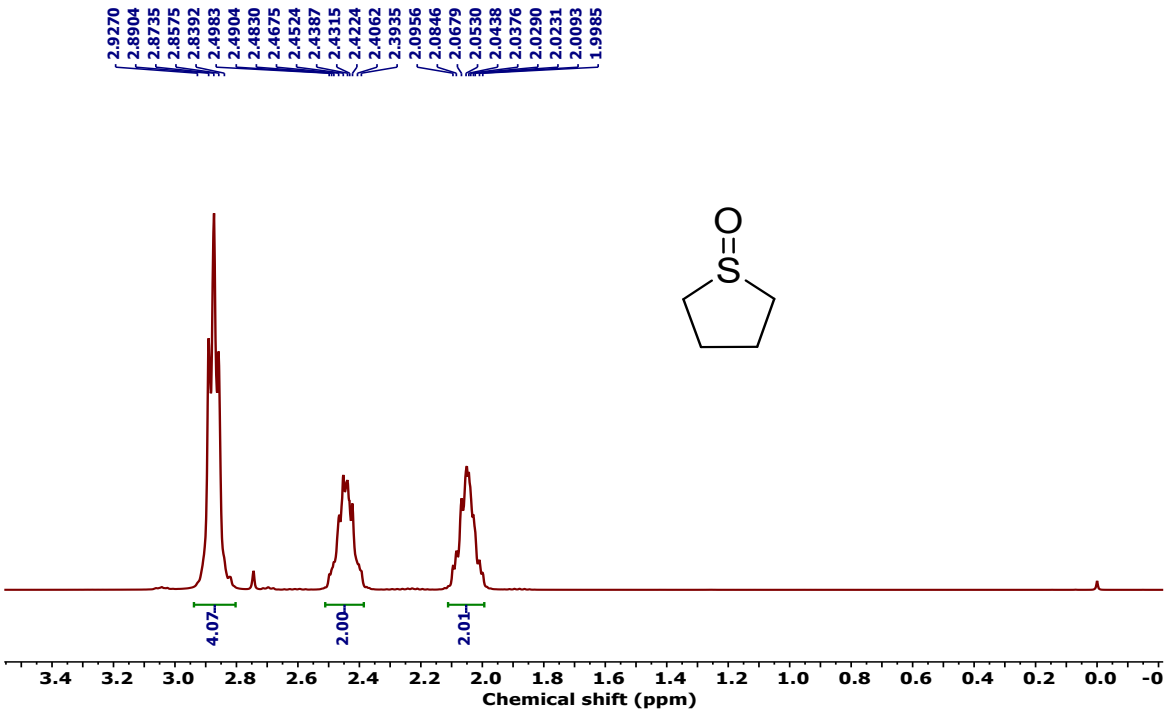

Fig. S37 ^{1}H NMR of Tetramethylene sulfoxide ($CDCl_3$, r.t.)

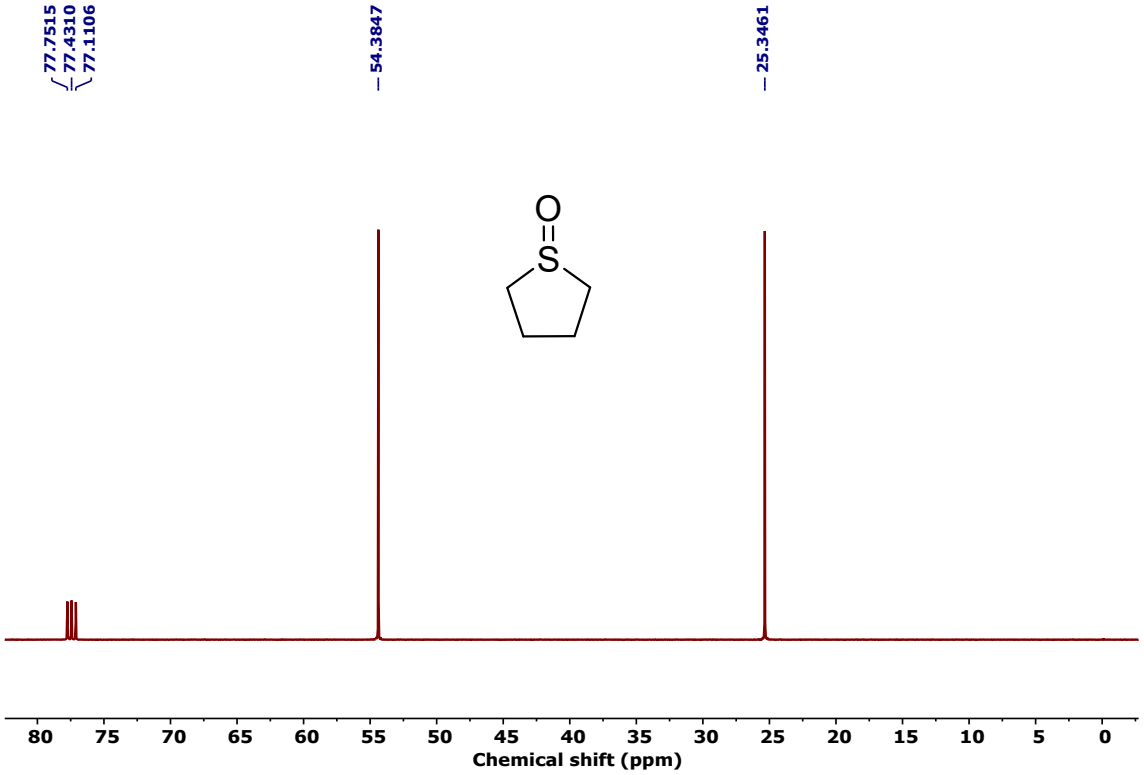

Fig. S38 ^{13}C NMR of Tetramethylene sulfoxide ($CDCl_3$, r.t.)

References

1 D.-Y. Zheng, E.-X. Chen, C.-R. Ye and X.-C. Huang, *J. Mater. Chem. A*, 2019, **7**, 22084–22091.
2 H. Wei, Z. Guo, X. Liang, P. Chen, H. Liu and H. Xing, *ACS Appl. Mater. Interfaces*, 2019, **11**, 3016–3023.
3 L. Liu, B. Zhang, X. Tan, D. Tan, X. Cheng, B. Han and J. Zhang, *Chem. Commun.*, 2020, **56**, 4567–4570.
4 Y. Qian, D. Li, Y. Han and H.-L. Jiang, *J. Am. Chem. Soc.*, 2020, **142**, 20763–20771.
5 X.-N. Zou, D. Zhang, T.-X. Luan, Q. Li, L. Li, P.-Z. Li and Y. Zhao, *ACS Appl. Mater. Interfaces*, 2021, **13**, 20137–20144.
6 H. Li, X. Li, J. Zhou, W. Sheng and X. Lang, *Chinese Chemical Letters*, 2022, **33**, 3733–3738.
7 M.-H. Hsieh, Z.-H. Su, E.-T. Wu and M. H. Huang, *ACS Appl. Mater. Interfaces*, 2023, **15**, 11662–11669.
8 L.-Q. Wei and B.-H. Ye, *ACS Appl. Mater. Interfaces*, 2019, **11**, 41448–41457.
9 W. Zhao, C. Yang, J. Huang, X. Jin, Y. Deng, L. Wang, F. Su, H. Xie, P. K. Wong and L. Ye, *Green Chem.*, 2020, **22**, 4884–4889.
10 Q. Zhu, H. An, T. Xu, S. Chang, Y. Chen, H. Luo and Y. Huang, *Applied Catalysis A: General*, 2023, **662**, 119283.
11 S. Liu, H. Yang, Y. Zhang, F. Wang, Q. Qin, D. Wang, C. Huang and Y.-Y. Zhang, *Journal of Colloid and Interface Science*, 2024, **663**, 919–929.
12 X. Lang, J. Zhao and X. Chen, *Angewandte Chemie International Edition*, 2016, **55**, 4697–4700.
13 J. Wang, Y. Liu, Z. Yuan, L. Li, P. Ma, J. Wang and J. Niu, *Chemistry – A European Journal*, 2024, **30**, e202303401.
14 C. Wang, Z. Xie, K. E. deKrafft and W. Lin, *J. Am. Chem. Soc.*, 2011, **133**, 13445–13454.
15 B. Zhang, J. Li, B. Zhang, R. Chong, R. Li, B. Yuan, S.-M. Lu and C. Li, *Journal of Catalysis*, 2015, **332**, 95–100.
16 Q. Li, X. Lan, G. An, L. Ricardez-Sandoval, Z. Wang and G. Bai, *ACS Catal.*, 2020, **10**, 6664–6675.
17 X. Lan, J. Wang, Q. Li, A. Wang, Y. Zhang, X. Yang and G. Bai, *ChemSusChem*, 2022, **15**, e202102455.
18 L. Liu, R. Song, Y. Wu, X. Song, J. Song, M. Chen, Y. Nie, C. Wang and J. Wan, *Journal of Colloid and Interface Science*, 2024, **663**, 775–786.
19 X. Li, Y. Wang, F. Zhang and X. Lang, *Journal of Colloid and Interface Science*, 2023, **648**, 683–692.
20 H. Shan, D. Cai, X. Zhang, Q. Zhu, P. Qin and J. Baeyens, *Chemical Engineering Journal*, 2022, **432**, 134288.
21 C. Su, R. Tandiana, B. Tian, A. Sengupta, W. Tang, J. Su and K. P. Loh, *ACS Catal.*, 2016, **6**, 3594–3599.
22 Y. Li, T.-X. Luan, K. Cheng, D. Zhang, W. Fan, P.-Z. Li and Y. Zhao, *ACS Materials Lett.*, 2022, **4**, 1160–1167.
23 Z. J. Wang, S. Ghasimi, K. Landfester and K. A. I. Zhang, *Chem. Commun.*, 2014, **50**, 8177–8180.
24 X. Chen, K. Deng, P. Zhou and Z. Zhang, *ChemSusChem*, 2018, **11**, 2444–2452.
25 J. Jiang, Z. Liang, X. Xiong, X. Zhou and H. Ji, *ChemCatChem*, 2020, **12**, 3523–3529.